# Surface Structure, Adsorption and Reaction on $TiO_2$(001) in the Atomic Scale Studied by Scanning Tunneling Microscopy and Temperature Programmed Desorption

# 走査トンネル顕微鏡と昇温脱離法による $TiO_2$(001)表面の原子レベル構造と分子吸着および反応性に関する研究

Ryugo TERO
[手老　龍吾]

# Contents

*Chapter 1.*

# Introduction

# 1. Introduction

## 1.1 General Introduction

Surface science on metal oxides is one of subjects with keenest attentions. Metal oxide is a versatile material applied to many industrial fields, such as catalyst including photocatalyst and environmental catalyst, gas sensor, coating against corrosion and rusty, pigment both for cosmetics and paints, electronic device and high-temperature superconductor. [1,2] For the sake of progress and new discoveries in these fields, understanding the property of metal oxide surfaces is an essential issue. The number of the studies about metal oxide surfaces is rapidly increasing due to importance as material.[1]

Surface science in itself is a relatively new scientific field and rapidly progressed in the recent three decades, though the first research related to surface has been already performed by M. Faraday in 1833; the catalytic effect of Pt for reaction of hydrogen and oxygen to water. Great development of ultra high vacuum (UHV) technology in 1970s made it possible to prepare a clean and well-ordered surface on a single crystal and to obtain well reproducible and reliable experimental data. Various physical techniques were devised in order to investigate the surfaces. Electron spectroscopy, such as X-ray photoelectron spectroscopy (XPS) and Auger electron spectroscopy, as well as diffraction method provided the information about electronic state and long range structure of the surface. Study on metal oxide single crystal was first reported in 1976,[3,4] and progressed with surface science experimental methods. However, it can not be denied that the surfaces of metal oxides have been less eagerly studied relative to metal and semiconductor surfaces for long time, partly because of difficulty in preparing a homogeneously well-ordered surface structure.

Surface "chemistry" has been strongly motivated and advanced from interest in catalysis. A large number of studies were performed about surface structure of metal single crystals and interaction with adsorbed species. Profitable information about the relation between surface structure, adsorption state of molecules and reactivity has been obtained.[5-7] However, in catalytic reactions, breaks of periodicity such as point defect multiple defect, step and kinks play important roles.[8-10] Especially on metal oxide surfaces, local conditions of surface atoms determine the property of each atom, such as ionicity, valence, and moreover, reactivity. Approaches to catalytic field with macroscopic surface science techniques somehow seemed to gradually decline because only averaged information from wide area could be obtained by spectroscopic and diffraction methods.

A sensational breakthrough has come in 1982. Binnig and Rohrer reported the first successive image of scanning tunneling microscopy (STM) with an unprecedented resolution in real space on atomic scale.[11] Each Si atom on Si(111)-(7×7) surface is clearly resolved.[11,12] Spatial resolution of 0.1 nm give the perspective to investigate dynamics of structure and adsorption species on specific site in atomic scale. STM was immediately applied to monitoring metal surfaces; a clean surface at first,[13] and then reconstructed surface induced by adsorbates.[14-17]

Excellent studies about molecular adsorption and reaction on single crystal surfaces by means of STM has been reported in succession. Restructuring and self-organization during reaction on metal surfaces was directly visualized by STM in real space, in real time.[18,19] The movements of domain boundaries with proceeding of reaction (oxidation of CO and $H_2$ on Pt(111)[19]) were clearly observed. The active site for dissociative chemisorption of nitric oxide, which is a decisive step in the catalytic reduction of nitric oxide, has been distinctly identified to single height steps on Ru(0001).[20,21] Nitrogen atoms partially distributed near steps right after NO exposure at 300 K and gradually

diffused to middle of terraces.[20] Time resolution of STM has also been improved. High scanning-speed STM with an ability of at most 20 images $s^{-1}$, fast enough to follow diffusion of oxygen atoms on Ru(0001) at room temperature (RT), was reported.[22] Somorjai and Salmeron has developed a high-pressure STM to overcome the "pressure gap" between UHV systems and actual catalytic conditions. Characteristic adlayers of individual adsorption and coadsorption of CO and NO appeared on Rh(111) surface at 0.05-700 Torr, which were not observed below $10^{-3}$ Pa, which was ordinal upper limit of pressure in UHV system.[23-26]

A recent preeminent application of STM is the vibrational spectroscopy to single molecule utilizing inelastic tunneling spectroscopy (IETS) between the tip and sample.[27] When a sample bias larger in absolute value than energy of physical mode, such as vibration, rotation and lateral movement, is applied, a new tunneling path to excite the mode opens additional to normal vacuum tunneling (elastic tunneling).[28-30] Vibrational spectroscopy to single molecule has become possible by investigating the critical energy to excite vibrational mode using a STM tip with atomic resolution. Actually second harmonic of tunneling current was detected by means of lock-in-amplifier.[27] Excitation of vibration can also lead to breaking or making bonds, which means reaction of the molecule. Induction of a reaction and characterization of reactant and product of the reaction to the target molecule are totally possible for STM-IETS.[31-35] Theoretical explanation of STM-IETS is still under controversy, but resonant transition is regarded as a convincing path.

Beside, principle of STM has employed to probe two-dimensional distribution of various physical values with high special resolution, for example atomic force microscopy (AFM), frictional force microscopy (FFM), magnetic force microscopy (MFM), Kelvin Force microscopy (KFM) and scanning near-field optical microscopy (SNOM). Nowadays these scanning probe microscopy methods are regarded as the indispensable

technology for nanotechnology, one of the destinations in next generation.[36]

STM observation of metal oxide surfaces is rather difficult because of large band gap and small electron conductivity. First successive STM observation of a metal oxide surface with atomic resolution was obtained on BiO plane of $Bi_2Sr_2CaCu_2O_{8+\delta}$, a layered superconductor material, cleaved under UHV.[37] However in 1990s number of STM studies on metal oxide surfaces with semiconductor property were rapidly increased.[38,39]

$TiO_2$ is a typical transitional metal oxide and has been widely used in many types of technology. One of the most important applications is catalyst. Originally $TiO_2$ had been studied as catalytic support of many reactions, moreover discovery of photocatalytic splitting of water on $TiO_2$ electrode made the number of studies burst out increasing.[40] The surface of $TiO_2$ single crystal is the best-investigated among metal oxide surfaces. Understanding and determination of surface structures and active sites control of active sites are the most important themes, which lead to catalysis control and design. Previous works on $TiO_2$ low-index planes to date about surface structure, molecular adsorption and reactivity are concisely summarized in section 1.3.

## 1.2 Purpose in This Thesis

In this thesis, I challenged to construct a new structure on $TiO_2$ single crystal valuable as adsorption and reaction field and to clarify its chemical characteristic. The goal of this work is to determine the structure and activity of the new phase in atomic scale. I chose (001) surface out of low index planes of $TiO_2$. The structure of $TiO_2$(001) is still unknown as will be described in section 1.3.2, therefore the structure in itself is a great interest. In chapter 3, surface morphology of $TiO_2$(001) depending on sample treatment is

described. I have investigated the surface structure of $TiO_2(001)$ surface by low energy electron diffraction (LEED) and STM varying cleaning conditions. The surface was easily turned into facet or disordered structure, but finally I succeeded in constructing an atomically ordered flat structure and visualizing by STM for the first time. In chapter 4, the new structure on $TiO_2(001)$ is examined in detail by means of LEED and STM. We named the new structure "bleachers-like structure" associated with the STM images. LEED pattern and its energy dependence indicated the structure was corresponding to one of previously reported phases, but high-resolution STM images could not been explained by the proposed model. Therefore a new structural model was constructed based on atom-resolved STM images. Adsorption sites of formic acid and methanol were adopted as a probe to verify the validity of the structural model. Both of STM images and molecular adsorptions indicate existence of two kinds of coordinatively unsaturated Ti cation. They were assigned to fivefold and fourfold coordinated Ti cations on the new structural model. In chapter 5, adsorption and reaction of methanol and acetic acid on the bleachers-like structure are investigated by STM and TPD. The activity of two kinds of Ti cations on the surface was evidently identified. The Ti cation assigned to fourfold coordination showed higher reactivity such as dissociative adsorption of decomposition of methoxy and acetate, on the other hand, Ti cation assigned to fivefold coordination had mild reactivity. The property of these sites was discussed comparing $TiO_2(110)$. In chapter 6, nano-scale structures on $TiO_2(001)$ are described. The unit cell of the bleachers-like structure assembled to pyramidal structure and flat terraces depending on conditions. Besides, surface morphology drastically changed from atomically ordered structure to outwardly disordered phase by reannealing at rather low temperature. Effect of molecular adsorption on structural transformation is also described.

## 1.3 Previous Studies about $TiO_2$ Single Crystal Surfaces

In this section, previous studies on $TiO_2$ single crystal surfaces are briefly summarized. Rutile $TiO_2$ surfaces are mostly described, but recent studies on anatase $TiO_2$ surfaces are also presented. At first, I would like to start with bulk property of rutile TiO2 crystal as fundamental issue.

### 1.3.1 Crystal Structure and Bulk Property of Rutile $TiO_2$

Rutile $TiO_2$ is composed of a unit cell with size of $0.459 \times 0.459 \times 0.296$ nm$^3$. Each $Ti^{4+}$ is surrounded by six $O^{2-}$ at slightly distorted octahedral site. The rutile structure can be considered as build up with the $TiO_6$ octahedra corner-sharing along the [110] and [1$\bar{1}$1] directions, and edge-sharing along the [001] direction. Therefore, the structure has anisotropy between the [100] (or [010]) and the [001] directions.[41]

Stoichiometric rutile $TiO_2$ is an insulator with a band gap of 3.05 eV. However $TiO_{2-x}$ ($n=10^{-5}$-$10^{-3}$) after reduction, by for example vacuum annealing, becomes n-type semiconductor.[42,43] Reduction of the crystal produces $Ti^{3+}$ at interstitial site,[44] which plays the role of donor. This conductive character makes it possible to perform many electron spectroscopic and diffraction methods and moreover STM on $TiO_2$ surfaces, preventing charge-up and conducting tunneling current. Assignment of the defect to whether interstitial titanium cations or oxygen defects was under controversy in early days,[45-50] and the former was interpreted as predominant species at present. $Ti^{3+}$ also works as a color center. Slightly yellowish stoichiometric $TiO_2$ crystal turns into light gray at first through light blue, deep blue and finally dark gray.[43,51] It is the simplest index to estimate the

degree of reduction. Electron conductivity of 0.8 Ω cm at 83 K was reported for $TiO_2$ pre-annealed at 973 K with charge carrier density of $4.5\text{-}5.8\times 10^{17}$ $cm^{-3}$.[43]

Diffusion of metal cations including titanium was plentifully studied formerly. Diffusion of impurity metal cations generally showed significant anisotropy between the [001] and perpendicular direction such as [100] and [110], which was explained by that void octahedral sites ranged along the [001] direction became open channels for diffusion.[52-57] For the most extreme example, $Li^+$ diffusion perpendicular to [001] was smaller than that parallel to [001] by a factor of at least $10^8$ up to 823 K.[53] However, only small anisotropy was appeared for self-diffusion of Ti (and O as well).[58-66]

### 1.3.2 $TiO_2$(110)

$TiO_2$(110) surface is the most extensively studied surface among not only on $TiO_2$ single crystal surfaces, but also all of metal oxide surfaces. Structure and electronic properties of $TiO_2$(110) were well-defined by various experimental techniques, such as LEED,[67-72] STM, [51,69,72-115], AFM,[116-121] NC-AFM,[88,105,122-126] medium-energy backscattered electron diffraction (MEED),[127] surface X-ray diffraction (SXRD),[128] electron stimulated desorption ion angular distribution (ESDIAD),[129,130] impact collision ion scattering spectroscopy (ICISS),[131] static secondary ion mass spectroscopy (SSIMS),[132] ultraviolet photoelectron spectroscopy (UPS), [3,44,70,71,133,134] X-ray photoelectron spectroscopy (XPS),[70,132,134-141], electron energy loss spectroscopy (EELS),[135] Inverse photoelectron spectroscopy (IPS),[142] High-Resolution EELS (HREELS),[140,143] and theoretical calculations.[99,112,144-156]

A sharp $(1\times 1)$ diffraction pattern is observed by LEED after $Ar^+$-sputtering followed by annealing to 800-1100 K.[67-72] It was proved experimentally[127,128] and theoretically[147,155]

that the structure of $TiO_2(110)$-$(1\times1)$ surface is almost identical to one of bulk-terminated structure shown in figure 1.1a. Small relaxation of surface atoms less than 0.02 nm from bulk position is indicated by theoretical calculations[147,155] and SXRD result.[128]

The first report of successive STM observation on $TiO_2$ surface has achieved by Rohrer et al. on highly-reduced $TiO_2(110)$, which was annealed at 900 K under UHV for 36 h.[73] Lines of bright spots along the [111] and [113] directions originated from crystallographic shear (CS) planes were clearly observed.

Afterward STM observation of near-stoichiometric $TiO_2(110)$-$(1\times1)$ surface has achieved by several groups.[72,75,77,78] The sample was enough reduced to gain electron conductivity but not enough to form CS planes. After annealing the $Ar^+$-sputtered sample to 800-1100 K, bright rows running along the [001] direction were observed by STM in positive sample bias conditions, accompanying with a sharp $(1\times1)$ LEED pattern. An atom-resolved STM image of $TiO_2(110)$-(1x1) is shown in figure 1.2. As mentioned above, $TiO_2(110)$-$(1\times1)$ surface is almost identical to the bulk-terminated structure. One-dimensional rows of fivefold coordinated Ti and bridge O along the [001] direction are alternately arranged (figure 1.1a). It was a fundamental issue whether exposed Ti or bridging O generated the protrusion in figure 1.2. Bridging O atoms have larger physical height than exposed Ti (Figure 1.1a), but tunneling probability in positive sample bias conditions is increased on unoccupied state localized above exposed Ti. Onishi and Iwasawa have definitely proved the bright rows to be exposed Ti from adsorption site of formate anions.[72,76] Formate anions were selectively adsorbed on the bright rows, which meant exposed Ti cations were brightly visualized. The assignment was substantiated by theoretical simulations.[83,149] The orbital of Ti cation responsible for tunneling in STM images is $t_{2g}$ of Ti3d, which is 1 eV above Fermi energy ($E_F$), while $e_{3g}$ is at 4 eV above $E_F$.[142,157] In some cases lined bright spots additionally appeared in the dark rows in the

STM images obtained with quite low sample bias and high tunneling current.[86,94] It was proposed that bridging oxygen became visible when the tip was very close to the sample.

In figure 1.2, several bright spots were observed on dark rows. They have been assigned to oxygen defects at first.[87] Later, Suzuki et al. insisted the probability of surface hydroxyl from the results of proton exposure and removal by ESD.[106] It is a quite important issue because both of oxygen defect and surface hydroxyl play important roles in surface reactions. [139,158-163] The recent experimental and theoretical results have revealed that both of them existed on the surface and are similarly visualized by STM.[164]

In spite of high stability of $TiO_2(110)$-$(1\times1)$ surface, several kinds of surface reconstruction has been reported. $TiO_2(110)$-$(1\times2)$ reconstructed phase was observed by LEED and STM after annealing to 1200 K[72,75,82] or long-period annealing at 700-800 K.[70,71,78,86] The later reversed to $(1\times1)$ structure by reannealing above 800 K,[71,86] while the former transformation was irreversible.[72] STM images of $TiO_2(110)$- $(1\times2)$ showed that the surface consisted of "double strand rows". Onishi and Iwasawa presented $Ti_2O_3$ added row model as the structure of double strand,[72,75] which was entirely different from initially proposed missing row models.[71,78,82] $Ti_2O_3$ added-row model was supported by a theoretical calculation[149] and the results of other experimental methods, such as ESDIAD,[130] ICISS[131] and NC-AFM.[131] Pang et al. proposed another "missing unit" $Ti_3O_5$ model.[120] Bennett et al. have found that there are two kinds of string structure with different contrast in STM images.[97] Major brighter strand (BS) formed $(1\times2)$ domain and minor long darker strand (DS) run in the $(1\times1)$ domain. BS and DS were proposed to be modified $Ti_3O_5$ model and $Ti_2O_3$ added row model, respectively.[97,100] However, Takakusagi et al. has assigned BS to $Ti_2O_3$ model and DS to another new model based on atom-resolve STM images.[121] The assignment of major structure, BS, to $Ti_2O_3$ was verified by the recent theoretical calculation, which revealed that $Ti_2O_3$ added-row model was thermally most

stable among all of previously proposed models and models the authors thought of.[145]

For structural formation and reconstruction on $TiO_2$ surfaces, diffusion of interstitial $Ti^{n+}$ ($n \leq 3$) between bulk and surface is a crucial factor. Several STM investigations recently revealed that surface structure of $TiO_2(110)$ drastically changed by annealing the surface in the presence of oxygen atmosphere depending on the conditions.[51,84,85,91,97,99,100,104,109] Growth of hill-like structures and $Ti_2O_3$ rows over $TiO_2(110)$-$(1\times1)$ terraces and transformation into a new $(1\times1)$ terraces by annealing at 800 K under $1\times10^{-5}$ Pa of oxygen was observed *in-situ*.[84,85] "Rosette" structure and $Ti_2O_3$ rows were formed on the surface after annealing between 500-660 K under $1\times10^{-4}$ Pa of oxygen.[91] The driving force of structural transformation on the surface was suggested to be the reaction of oxygen with $Ti^{n+}$ diffused to the surface, forming the added layer of $TiO_x$. Diffusion rate and density of interstitial Ti, annealing temperature and oxygen pressure are the principal parameters for the structural transformation. Henderson has investigated the self-diffusion of Ti and O between bulk and surface by means of SSIMS and revealed two ways for self-diffusion; slow diffusion of both of Ti and O between surface at 400-700 K, and fast diffusion of Ti into bulk above 700 K.[132] Likewise, on $TiO_2(001)$ reoxidation of $Ar^+$-sputtered surface self-diffusion occurred above 560 K.[165,166] As described in 1.3.1, interstitial Ti isotropically diffuse in bulk. The results are reasonable to interpret the drastic change of $TiO_2(110)$ due to diffusion of interstitial Ti cations.

Molecular adsorption and reaction on $TiO_2(110)$ have also been extensively studied by various experimental techniques and theoretical calculations:
HCOOH,[72,76,79-81,101,133,167-181] $CH_3COOH$,[181-184] $C_6H_5COOH$,[183] $(CH_3)_3CCOOH$,[185] HC=COOH, $CHF_2COOH$, $CF_3COOH$,[181] $H_2CO$,[158] $CH_3OH$,[133,162,186-191] $C_2H_5OH$,[191,192] $CH_3SH$[193] CO,[139] $CO_2$,[139,194-196] $SO_2$,[133,197] NO,[158,198] $CH_3Cl$,[159,199] $H_2O$,[110,158,164,188,189,195,200-203] Hydrogen,[106,139,202] pyridine and its derivatives,[204,205]

$[Rh^{I}(CO)_2Cl]_2$,[206,207] $Rh(acac)_2CH$,[207] $O_2$,[103,132,139,161,180,200 136,160,202] Cl,[208-210] and S.[211,212]

Formic acid is the simplest organic molecule and therefore the most investigated on $TiO_2(110)$. At RT formic acid dissociatively adsorbed on $TiO_2(110)$ as bridging formate anion forming $(2\times 1)$ overlayer at saturation coverage of 0.5 ML.[76,133,167,168,172] Other kinds of carboxylic acid similarly adsorb on $TiO_2(110)$ as corresponding carboxylate.[181-185] Theoretical calculations have shown that surface formate is stabilized by coadsorbed hydroxyl at neighboring bridging oxygen.[173,174] In the thermal reaction of saturated coverage of $DCOO^-$ on $TiO_2(110)$, 20 % of adsorbed formate desorbed as DCOOD at 350 K recombining with surface hydroxyl and the other unimolecularly decomposed at 570 K releasing CO, $CO_2$, $D_2$, $D_2O$ and DCOOD. It has been indicated that formate decomposition contains complex mechanisms.[178]

The defect site of bridging oxygen is regarded as an important active site for various reactions. It has been reported that dissociative adsorption of $H_2O$, $CH_3OH$ and $O_2$ occurred only on the defect site and did not on perfect $(1\times 1)$ surface.[139,159-162,164] Oxygen defect site worked as active site of bimolecular deoxygenation of $D_2O$, $H_2CO$ and NO to $D_2$, $C_2H_4$ and $N_2O$, respectively.[158] $Ti^{3+}$ cation in the defect site after removal of oxygen was considered to be crucial for these reactions.

### 1.3.3 $TiO_2(001)$

In contrast with $TiO_2(110)$ surface, extremely little is known about $TiO_2(001)$ surface. Experimental results heretofore reported about $TiO_2(001)$ are LEED,[67,68,213,214] UPS,[44,215,216] XPS,[165,215,217] ESDIAD,[129] NEXAFS,[166] Ion scattering spectroscopy (ISS),[217] reflection electron microscopy (REM),[218] STM,[219-223] and AFM.[116-118,222,224] Figure 1.1b shows the bulk-terminated structural model of $TiO_2(001)$. All of Ti atoms on the surface

have fourfold coordination, doubly uncoordinated comparing with Ti atoms in the bulk. The surface is non-polar but quite unstable due to low ligand coordination of the surface atoms. Theoretical calculations has revealed the highest surface energy among the low-index planes of $TiO_2$ single crystal, such as (110) and (100), and predicted surface reconstruction from bulk terminated structure.[144,147,150,151,153,155]

In fact, two ordered phases has been observed by LEED.[68,213] Long annealing periods for hours at 900 K after $Ar^+$-sputtering produced a sharp pattern, and long annealing at 1400 K or above resulted in another sharp pattern.[213] The values of the temperature were afterward pointed out to be overestimated due to an apparatus problem and actually ~750 K and ~950 K for lower- and higher- temperature phase, respectively.[225] The subspots of both two phases did not simply converge on the specular direction with increase of incident beam energy, which was the symptomatic behavior of faceted surfaces. Firment analyzed the movement of subspots between the beam energy of 24-90 eV and searched for the specular beam of the facet planes. The tilted angle from (001) plane was estimated to be ~33 ° for the former and 13 ° for the later. The lower and the higher temperature phases were assigned to {011}-faceted structure with $(2\times 1)$ reconstruction and {114}-faceted structure, respectively. Such kinematic LEED analysis is valuable for determination of facet plane and long-range periodicity, but valueless for atomic scale structure. Firment displayed bulk-terminated (011) and (114) surface structural model as tentative illustration in ref. [213] because no information about reconstruction could be obtained. However, these two drawings of bulk-terminated structures are the only proposal for the surface structure of $TiO_2$(001) and accepted to date because no further information has been obtained.

The first trial for STM observation of the two phases has reported by Poirier et al.[219] Annealing under UHV at 783 K for 2 h after $Ar^+$-sputtering resulted in large facet structures

with width of several tens nm. The facet planes were mainly corresponding to (011) and its similarities such as (045) and (023). Some (114) and (111) facet planes were also observed. Following AFM studies also have shown large scale faceted or disordered structures. Antonik et al. reported a complex surface morphology consisting of a large distribution of facet sizes and orientations for the lower temperature phase, which was prepared by annealing at 1173 K for 1-4 hours (the temperature would be overestimated).[116-118] Watson and Barteau reported that all of $Ar^+$-ion-bombarded surface, lower-temperature phase and higher-temperature phase were similarly composed of large flat plateaus ranging in size from 21 to 75 nm.[224] No structural information in atomic scale has obtained up to the present for neither lower- nor higher-temperature phase.

Recently, one more phase has been reported to appear under non-equilibrium conditions. After annealing above 1473 K with the heating and cooling rate of 100 K $s^{-1}$, network-like structures with periodicity of $\left(7\sqrt{2}\times\sqrt{2}\right)$ was observed by STM and RHEED.

Distinct electronic feature of $TiO_2$(001) from other surfaces has been reported by UPS. A small defect state due to interstitial $Ti^{3+}$ was detected in the band gap, ~1.0 eV below Fermi, only on $TiO_2$(001) among vacuum-fractured $TiO_2$ (110), (100) and (001) surfaces.[44] $Ti^{3+}$ was originated from oxygen desorption so that it is comparable with the ESD result that oxygen more easily desorbs from $TiO_2$(001) than $TiO_2$(110). The difference may also be related to higher surface energy of $TiO_2$(001) on which all oxygen atoms have twofold coordination in the bulk-terminated structure.

Low ligand coordination of surface atoms and maybe due to the characteristic electronic structure, unique reactivities arise on $TiO_2$(001). In spite of ignorance of surface structure, rather large number of studies about reactivity of $TiO_2$(001) has been reported.[191,216,225-244] Many of the works were carried out by Barteau et al.. Each of

$Ar^+$-sputtered, lower-temperature phase and higher-temperature phase showed different reactivity in TPD. Aliphatic alcohols unimolecularly reacted to form corresponding aldehydes and hydro carbons on the lower-temperature phase.[225,230] Additional bimolecular reaction product, ether, desorbed from the higher-temperature phase.[225] The active sites of unimolecular and bimolecular reaction were assigned to fivefold and fourfold coordinated $Ti^{4+}$, respectively, based on the {011}- and {114}-faceted structural models proposed in ref. [213] (figure 1.3). Only fivefold coordinated Ti was exposed on the {011}-faceted structural model, while both of fourfold and fivefold coordinated Ti existed on the {114}-faceted structural model. Fourfold coordinated Ti with two adsorbed methoxy was proposed as the reaction intermediate state for bimolecular ether synthesis. The concept was comparable with TPD of carboxylic acids. Ketene and additional ketone desorbed from lower- and higher-temperature phase, respectively and doubly adsorbed carboxylate on fourfold coordinated Ti was assigned to the intermediate of the bimolecular ketonization.[234] However, {011}- and {114}-faceted structural model were bulk-terminated structural models, tentative illustrations with no consideration for surface reconstruction, as described above.[213] It seems also inconsistent with that no bimolecular reaction product is detected form $Ar^+$-sputtered surface,[225,230,234] on which various kinds of Ti cations different in coordination number and valence remained.[165]

### 1.3.4 Other Surfaces of Rutile $TiO_2$

The structure of $TiO_2$(100) surface, which is not equivalent to (001) surface, has been well-defined though the number of study is not as large as $TiO_2$(110). $(1\times1)$, $(1\times3)$, $(1\times5)$ and $(1\times7)$ patterns were observed by LEED with increasing annealing temperature after $Ar^+$-sputtering.[67] The structure of $TiO_2$(100)-$(1\times1)$ is almost identical to

bulk-terminated structure shown in figure 1.1c, and corresponding STM images has been reported.[245] $TiO_2(100)$-$(1\times3)$ surface is composed of serrated (110)-micro facets.[246,247] $TiO_2(100)$-$(1\times3)$ as well as two intermediate $(1\times3)$ phases from $(1\times1)$ to $(1\times3)$ was observed by STM and NC-AFM.[105,245,248,249] Adsorption and reaction of $O_2$, $CO_2$, $H_2O$,[250] HCOOH,[251] and $CH_3OH$[190] were reported. Other surfaces which STM images with atomic resolution has been achieved were $TiO_2(111)$[107] and $TiO_2(210)$[252].

### 1.3.5 Anatase $TiO_2$

Anatase $TiO_2$ (a-$TiO_2$) is also used popularly in photocatalytic and non-photoinduced reactions. In many (but not all) cases anatase shows higher photocatalytic activity than rutile partly due to 0.2 eV larger bandgap.[253,254] Surface science approaches to a-$TiO_2$ surfaces is just at beginning. Theoretical calculations have revealed that the (101) surface of anatase is thermodynamically most stable.[255,256] Preparation of anatase-type $TiO_2$ surface is difficult because normal thermal treatment can result in transformation to rutile structure. Well-ordered a-$TiO_2(001)$ and (101) surfaces were obtained by MOCVD on $SrTiO_3(001)$,[257,258] oxygen-plasma-assisted molecular beam epitaxy (OPA-MBE)[259,260] on $SrTiO_3(001)$ and OPA-MBE on anatase $TiO_2(101)$ single crystal, respectively.[261] LEED investigations at first stage have shown a-$TiO_2(101)$-$(1\times1)$ and a-$TiO_2(001)$-$(1\times4)$ patterns.[257,258,262] A-$TiO_2(101)$-$(1\times1)$ surface was assigned to almost identical structure to bulk-termination from atom-resolved STM images.[261] On a-$TiO_2(001)$-$(1\times4)$, so called "added molecule" structure was proposed, which was in agreement with high resolution STM and NC-AFM images.[259,260] Reactivity of a-$TiO_2(001)$-$(1\times4)$ was also investigated in ref. [260], however no product was detected in TPD of formic acid and acetic acid from perfect a-$TiO_2(001)$-$(1\times4)$ surface. It may be due

to a problem of surface preparation in my personal opinion. Oxygen adsorption from residual oxygen of OPA-MBE would result in deactivation of the surface.

**References**


(1) Henrich, V. E.; Cox, P. A. *The Surface Science of Metal Oxides*; Cambridge University Press: Cambridge, 1996.

(2) Iwasawa, Y. *Stud. Surf. Sci. Catal.* **1996**, *101*, 21-34.

(3) Henrich, V. E.; Dresselhaus, G.; Zeiger, H. J. *Phys. Rev. Lett.* **1976**, *36*, 1335-1339.

(4) Powell, R. A.; Spicer, W. E. *Phys. Rev. B* **1976**, *13*, 2601-2604.

(5) Weldon, M. K.; Friend, C. M. *Chem. Rev.* **1996**, *96*, 1391-1411.

(6) Bent, B. E. *Chem. Rev.* **1996**, *96*, 1361-1390.

(7) Goodman, D. W. *Chem. Rev.* **1995**, *95*, 523-536.

(8) Taylor, H. S. *Proc. Roy. Soc. A* **1925**, *108*, 105-111.

(9) Somorjai, G. A.; Joyner, R. W.; Lang, B. *Proc. Roy. Soc. A* **1972**, *331*, 335-346.

(10) Somorjai, G. A. *Chemistry in Two Dimensions: Surfaces*; Cornell University Press: Ithaca, 1981.

(11) Binnig, G.; Rohrer, H. *Helv. Phys. Acta.* **1982**, *55*, 726-735.

(12) Binnig, G.; Rohrer, H.; Gerber, C.; Weibel, E. *Phys. Rev. Lett.* **1983**, *50*, 120-123.

(13) Hallmark, V. M.; Chiang, S.; Rabolt, J. F.; Swalen, J. D.; Wilson, R. J. *Phys. Rev. Lett.* **1987**, *59*, 2879-2882.

(14) Gritsch, T.; Coulman, D.; Behm, R. J.; Ertl, G. *Phys. Rev. Lett.* **1989**, *63*, 1086-1089.

(15) Kuk, Y.; Chua, F. M.; Silverman, P. J. *Phys. Rev. B* **1990**, *41*, 12393-12402.

(16) Jensen, F.; Besenbacher, F.; Laegsgaard, E.; Stensgaard, I. *Phys. Rev. B* **1990**, *42*, 9206-9209.

(17) Coulman, D. J.; Wintterlin, J.; Behm, R. J.; Ertl, G. *Phys. Rev. Lett.* **1990**, *64*, 1761-1764.

(18) Ertl, G. *J. Mol. Catal.* **1992**, *74*, 1-9.

(19) Ertl, G. *Chemical Record* **2001**, *1*, 33-45.

(20) Zambelli, T.; Trost, J.; Wintterlin, J.; Ertl, G. *Phys. Rev. Lett.* **1996**, *76*, 795-798.

(21) Zambelli, T.; Wintterlin, J.; Trost, J.; Ertl, G. *Science* **1996**, 1688-1690.

(22) Renisch, S.; Schuster, R.; Wintterlin, J.; Ertl, G. *Phys. Rev. Lett.* **1999**, *82*, 3839-3842.

(23) Rider, K.; Hwang, K. S.; Salmeron, M.; Somorjai, G. A. *J. Am. Chem. Soc.* **2002**, *124*, 5588-5593.

(24) Rider, K. B.; Hwang, K. S.; Salmeron, M.; Somorjai, G. A. *Phys. Rev. Lett.* **2001**, *86*, 4330-4333.

(25) Cernota, P.; Rider, K.; Yoon, H. A.; Salmeron, M.; Somorjai, G. A. *Surf. Sci.* **2000**, *445*, 249-255.

(26) Jensen, J. A.; Rider, K. B.; Chen, Y.; Salmeron, M.; Somorjai, G. A. *J.Vac.Sci.Technol. B* **1999**, *17*, 1080-1084.

(27) Stipe, B. C.; Rezaei, M. A.; Ho, W. *Science* **1998**, *280*, 1732-1735.

(28) Lauhon, L. J.; Ho, W. *J. Chem. Phys.* **1999**, *111*, 5633-5636.

(29) Stipe, B. C.; Rezaei, M. A.; Ho, W. *Phys. Rev. Lett.* **1998**, *81*, 1263-1266.

(30) Ho, W. *Acc. Chem. Res.* **1998**, *31*, 567-573.

(31) Gaudioso, J.; Lee, H. J.; Ho, W. *J. Am. Chem. Soc.* **1999**, *121*, 8479-8485.

(32) Lauhon, L. J.; Ho, W. *J. Phys. Chem. A* **2000**, *104*, 2463-2467.

(33) Lauhon, L. J.; Ho, W. *Phys. Rev. Lett.* **2000**, *84*, 1527-1530.

(34) Lee, H. J.; Ho, W. *Science* **1999**, *286*, 1719-1722.

(35) Lauhon, L. J.; Ho, W. *Surf. Sci.* **2000**, *451*, 219-225.

(36) Nyffenegger, R. M.; Penner, R. M. *Chem. Rev.* **1997**, *97*, 1195-1230.

(37) Kirk, M. D.; Nogami, J.; Baski, A. A.; Mitzi, D. B.; Kapitulnik, A.; Geballe, T. H.; Quate, C. F. *Science* **1988**, *242*, 1673-1675.

(38) Leibsle, F. M.; Murray, P. W.; Condon, N. G.; Thornton, G. *J. Phys. D: Appl. Phys.* **1997**, *30*, 741-756.

(39) Egdell, R. G.; Jones, F. H. *J. Mater. Chem.* **1988**, *8*, 469-484.

(40) Fujishima, A.; Honda, K. *Nature* **1972**, *238*, 37-38.

(41) Hyde, B. G.; Andersson, S. *Inorganic Crystal Structures*; Wiley Interscience: New York, 1989.

(42) Blumenthal, R. N.; Coburn, J.; Baukus, J.; Hirthe, W. M. **1966**.

(43) Breckenridge, R. G.; Hosler, W. R. *Phys. Rev.* **1953**, *91*, 793-802.

(44) Henrich, V. E.; Kurtz, R. L. *Phys. Rev. B* **1981**, *23*, 6280-6287.

(45) Kofstad, P. *J. Less-Common Metals* **1967**, *13*, 635-638.

(46) Sawatari, H.; Iguchi, E.; Tilley, R. J. D. *J. Phys. Chem. Solids* **1982**, *43*, 1147-1155.

(47) Yagi, E.; Koyama, A.; Sakairi, H.; Hasiguti, R. *J. Phys. Soc. Jpn.* **1977**, *42*, 939-946.

(48) Tannhauser, D. S. *Solid State Commun.* **1963**, *1*, 223-225.

(49) Barbanel', V. I.; Bogomolov, V. N.; Borodin, S. A.; Budarina, S. I. *Soviet Phys. Solid State* **1969**, *11*, 431-433.

(50) Millot, F.; Blanchin, M. G.; Tetot, R.; Marucco, J. F.; Poumellec, B.; Picard, C.; Touzelin, B. *Prog. Solid St. Chem.* **1987**, *17*, 263-293.

(51) Li, M.; Hebenstreit, W.; Diebold, U. *J. Phys. Chem. B* **2000**, *104*, 4944-4950.

(52) Steel, J. L.; McCartney, E. R. *Nature* **1969**, *222*, 79.

(53) Johnson, O. W. *Phys. Rev.* **1964**, *136*, A284-A290.

(54) Sasaki, J.; Peterson, N. L.; Hoshino, K. *J. Phys. Chem. Solids* **1985**, *46*, 1267-1283.

(55) Peterson, N. L.; Sasaki, J. *NATO ASI series B* **1985**, *129*, 269-284.

(56) Ruebenbauer, K.; Wdowik, U. D.; Kwater, M.; J.T., K. *Phys. Rev. B* **1996**, *54*, 12880-12891.

(57) Ajayi, O. B.; Nagel, L. E.; Raistrick, I. D.; Huggins, R. A. *J. Phys. Chem. Solids*

**1976**, *37*, 167-172.

(58) Akse, J. R.; Whitehurst, H. B. *J. Phys. Chem. Solids* **1978**, *39*, 457-465.

(59) Hoshino, K.; Peterson, N. L.; Wiley, C. L. *J. Phys. Chem. Solids* **1985**, *46*, 1397-1411.

(60) Lundy, T. S.; Coghlan, W. A. *J. Phys. (Paris), Colloq.* **1973**, *34*, C9-299.

(61) Huntington, H. B.; Sullivan, G. A. *Phys. Rev. Lett.* **1965**, *14*, 177-178.

(62) Iguchi, E.; Yajima, K. *J. Phys. Soc. Jpn.* **1972**, *32*, 1415-1421.

(63) Radecka, M.; P. Sobas, P.; Rekas, M. *Solid State Ionics* **1999**, *119*, 55-60.

(64) Haul, R.; Dumbgen, G. *J. Phys. Chem. Solids* **1965**, *26*, 1-10.

(65) Derry, D. J.; Lees, D. G.; Calvert, J. M. *J. Phys. Chem. Solids* **1981**, *42*, 57-64.

(66) Moore, D. K.; Cherniak, D. J.; Watson, E. B. *Am. Mineral.* **1998**, *83*, 700-711.

(67) Chung, Y. W.; Lo, W. J.; Somorjai, G. A. *Surf. Sci.* **1977**, *64*, 588-602.

(68) Tait, R. H.; Kasowski, R. V. *Phys. Rev. B* **1979**, *20*, 5178-5191.

(69) Zhong, Q.; Vohs, J. M.; Bonnell, D. A. *Surf. Sci.* **1992**, *274*, 35-43.

(70) Kao, C. C.; Tsai, S. C.; Bahl, M. K.; Chung, Y. W.; Lo, W. J. *Surf. Sci.* **1980**, *95*, 1-14.

(71) Moller, P. J.; Wu, M.-C. *Surf. Sci.* **1989**, *224*, 265-276.

(72) Onishi, H.; Fukui, K.; Iwasawa, Y. *Bull. Chem. Soc. Jpn.* **1995**, *68*, 2447-2458.

(73) Rohrer, G. S.; Henrich, V. E.; Bonnell, D. A. *Science* **1990**, *250*, 1239-1241.

(74) Rohrer, G. S.; Henrich, V. E.; Bonnell, D. A. *Surf. Sci.* **1992**, *278*, 146.

(75) Onishi, H.; Iwasawa, Y. *Surf. Sci.* **1994**, *313*, L783-L789.

(76) Onishi, H.; Iwasawa, Y. *Chem. Phys. Lett.* **1994**, *226*, 111-114.

(77) Novak, D.; Garfunkel, E.; Gustafsson, T. *Phys. Rev. B* **1994**, *50*, 5000-5003.

(78) Sander, M.; Engel, T. *Surf. Sci.* **1994**, *302*, L263-L268.

(79) Onishi, H.; Iwasawa, Y. *Jpn. J. Appl. Phys.* **1994**, *33*, L1338-L1341.

(80) Onishi, H.; Iwasawa, Y. *Langmuir* **1994**, *10*, 4414-4416.

(81) Yamaguchi, Y.; Onishi, H.; Iwasawa, Y. *J. Chem. Soc. Faraday Trans.* **1995**, *91*, 1663-1668.

(82) Murray, P. W.; Condon, N. G.; Thornton, G. *Phys. Rev. B* **1995**, *51*, 10989-10997.

(83) Diebold, U.; Anderson, J. F.; Ng, K.-O.; Vanderbilt, D. *Phys. Rev. Lett.* **1996**, *77*, 1322-1325.

(84) Onishi, H.; Iwasawa, Y. *Phys. Rev. Lett.* **1996**, *76*, 791.

(85) Onishi, H.; Iwasawa, Y. *Surf. Sci.* **1996**, *357/358*, 773-776.

(86) Xu, C.; Lai, L.; Zajac, G. W.; Goodman, D. W. *Phys. Rev. B* **1997**, *56*, 13464-13482.

(87) Diebold, U.; Lehman, J.; Mahmoud, T.; Kuhn, M.; Leonardelli, G.; Hebenstreit, W.; Schmid, M.; Varga, P. *Surf. Sci.* **1998**, *411*, 137-153.

(88) Iwasawa, Y. *Surf. Sci.* **1998**, *404-404*, 8-19.

(89) Kimura, S.; Tsukada, M. *Appl. Surf. Sci.* **1998**, *130-132*, 587-592.

(90) Lai, X.; Clair, T. P. S.; Valden, M.; Goodman, D. W. *Prog. Surf. Sci.* **1998**, *59*, 25-52.

(91) Li, M.; Hebenstreit, W.; Diebold, U. *Surf. Sci.* **1998**, *414*, L951-L956.

(92) Nörenberg, H.; Briggs, G. A. D. *Surf. Sci.* **1998**, *402-404*, 738-741.

(93) Nörenberg, H.; Tanner, R. E.; Schierbaum, K. D.; Fischer, S.; Briggs, G. A. D. *Surf. Sci.* **1998**, *396*, 52-60.

(94) Tanner, R. E.; Castell, M. R.; Briggs, G. A. D. *Surf. Sci.* **1998**, *412/413*, 672-681.

(95) Valden, M.; Lai, X.; Goodman, D. W. *Science* **1998**, *281*, 1647-1650.

(96) Zhang, L. P.; Li, M.; Diebold, U. *Surf. Sci.* **1998**, *412/413*, 242-251.

(97) Bennett, R. A.; Stone, P.; Price, N. J.; Bowker, M. *Phys. Rev. Lett.* **1999**, *82*, 3831-3834.

(98) Bennett, R. A.; Poulston, S.; Stone, P.; Bowker, M. *Phys. Rev. B* **1999**, *59*, 10341-10346.

(99) Li, M.; Hebenstreit, W.; Gross, L.; Diebold, U.; Henderson, M. A.; Jennison, D. R.; Schultz, P. A.; Sears, M. P. *Surf. Sci.* **1999**, *437*, 173-190.

(100) Stone, P.; Bennett, R. A.; Bowker, M. *New. J. Phys.* **1999**, *1*, 1.1-1.12.

(101) Bennett, R. A.; Stone, P.; Smith, R. D.; Bowker, M. *Surf. Sci.* **2000**, *454*, 390-395.

(102) Dulub, O.; Hebenstreit, W.; Diebold, U. *Phys. Rev. Lett.* **2000**, *84*, 3646-3549.

(103) Gan, S.; Liang, Y.; Bear, D. R. *Surf. Sci.* **2000**, *459*, L498-L502.

(104) Li, M.; Hebenstreit, W.; Diebold, U. *Phys. Rev. B* **2000**, *61*, 4926-4933.

(105) Pang, C. L.; Raza, H.; Haycock, S. A.; Thornton, G. *Appl. Surf. Sci.* **2000**, *157*, 233-238.

(106) Suzuki, S.; Fukui, K.; Onishi, H.; Iwasawa, Y. *Phys. Rev. Lett.* **2000**, *84*, 2156-2159.

(107) Uetsuka, H.; Sasahara, A.; Onishi, H. *Jpn. J. Appl. Phys.* **2000**, *39*, 3769-3772.

(108) Berko, A.; Biro, T.; Kecskes, T.; Solymosi, F. *Vacuum* **2001**, *61*, 317-322.

(109) Bowker, M.; Smith, R. D.; Bennett, R. A. *Surf. Sci.* **2001**, *478*, L309-L312.

(110) Brookes, I. M.; Muryn, C. A.; Thornton, G. *Phys. Rev. Lett.* **2001**, *87*, 266103-266101-266104.

(111) Iwasawa, Y.; Onishi, H.; Fukui, K. *Topics in Catal.* **2001**, *14*, 163-172.

(112) Jennison, D. R.; Dulub, O.; Hebenstreit, W.; Diebold, U. *Surf. Sci.* **2001**, *492*, L677-L687.

(113) Meier, D. C.; Rizzi, G. A.; Granozzi, G.; Lai, X.; Goodman, D. W. *Langmuir* **2002**, *18*, 698-705.

(114) Yin, D.; Komiyama, M. *Jpn. J. Appl. Phys.* **2001**, *40*, 4281-4284.

(115) Berko, A.; Solymosi, F. *J. Phys. Chem. B* **2000**, *104*, 10215-10221.

(116) Antonik, M. D.; Edwards, J. C.; Lad, R. J. *Mat. Res. Soc. Symp. Proc.* **1992**, *237*,

459-464.

(117) Lad, R. J.; Antonik, M. D. *Ceram. Trans.* **1991**, *1*, 359-367.

(118) Antonik, M. D.; Lad, R. J. *J. Vac. Sci. Technol. A* **1992**, *10*, 669-673.

(119) Fukui, K.; Sugiyama, S.; Iwasawa, Y. *Phys. Chem. Chem. Phys.* **2001**, *3*, 3871-3877.

(120) Pang, C. L.; Haycock, S. A.; Raza, H.; Murray, P. W.; Thornton, G.; Gulseren, O.; James, R.; Bullett, D. W. *Phys. Rev. B* **1998**, *58*, 1586-1589.

(121) Takakusagi, S.; Fukui, K.; Nariyuki, F.; Iwasawa, Y. *Surf. Sci., in press.*

(122) Fukui, K.; Onishi, H.; Iwasawa, Y. *Chem. Phys. Lett.* **1997**, *280*, 296-301.

(123) Hotsenpiller, P. A. M.; Bolt, J. D.; Farneth, W. E.; Lowekamp, J. B.; Rohrer, G. S. *J. Phys. Chem. B* **1998**, *102*, 3216-3226.

(124) Ashino, M.; Uchihashi, T.; Yokoyama, K.; Sugawara, Y.; Morita, S.; Ishikawa, M. *Appl. Surf. Sci.* **2000**, *157*, 212-217.

(125) Ashino, M.; Uchihashi, T.; Yokoyama, K.; Sugawara, Y.; Morita, S.; Ishikawa, M. *Phys. Rev. B* **2000**, *61*, 13955-13959.

(126) Ashino, M.; Sugawara, Y.; Morita, S.; Ishikawa, M. *Phys. Rev. Lett.* **2001**, *86*, 4334-4337.

(127) Maschhoff, B. L.; Pan, J. M.; Madey, T. E. *Surf. Sci.* **1991**, *259*, 190.

(128) Charlton, G.; Howes, P. B.; Nicklin, C. L.; Steadman, P.; Taylor, J. S. G.; Muryn, C. A.; Harte, S. P.; Mercer, J.; McGrath, R.; Norman, D.; Turner, T. S.; Thornton, G. *Phys. Rev. Lett.* **1997**, *78*, 495-498.

(129) Kurtz, R. L. *Surf. Sci.* **1986**, *177*, 526-552.

(130) Guo, Q.; Cocks, I.; Williams, E. M. *Phys. Rev. Lett.* **1996**, *77*, 3851-3854.

(131) Asari, E.; Hayami, W.; Souda, R. *Appl. Surf. Sci.* **2000**, *167*, 169-176.

(132) Henderson, M. A. *Surf. Sci.* **1999**, *419*, 174-187.

(133) Onishi, H.; Aruga, T.; Egawa, C.; Iwasawa, Y. *Surf. Sci.* **1988**, *193*, 33-46.

(134) Wang, L.-Q.; Baer, D. R.; Engelhard, M. H. *Surf. Sci.* **1994**, *320*, 295-306.

(135) Gopel, W.; Anderson, J. A.; Frankel, D.; Jaehnig, M.; Phillips, K.; Schafer, J. A.; Rocker, G. *Surf. Sci.* **1984**, *139*, 333-346.

(136) Shultz, A. N.; Jang, W.; Hetherington III, W. M.; Baer, D. R.; Wang, L.-Q.; Engelhard, M. H. *Surf. Sci.* **1995**, *339*, 114-124.

(137) Reis, S.; Krumm, H.; Niklewski, A.; Staemmler, V.; Woll, C. *J. Chem. Phys.* **2002**, *116*, 7704-7713.

(138) Bardi, U.; Tamura, K.; Owari, M.; Nihei, Y. *Appl. Surf. Sci.* **1988**, *32*, 352-362.

(139) Gopel, W.; Rocker, G.; Feierabend, R. *Phys. Rev. B* **1983**, *28*, 3427-3438.

(140) Guo, Q.; Lee, S.; Goodman, D. W. *Surf. Sci.* **1999**, *437*, 38-48.

(141) Patel, R.; Guo, Q.; Cocks, I.; Williams, E. M.; Róman, E.; deSegovia, J. L. *J. Vac. Sci. Technol. A* **1997**, *15*, 2553-2556.

(142) See, A. K.; Bartynski, R. A. *J. Vac. Sci. Technol. A* **1992**, *10*, 2591.

(143) Cox, P. A.; Egdell, R. G.; Eriksen, S.; Flavell, W. R. *J. Electron Spectros. Relat. Phenomena* **1986**, *39*, 117-126.

(144) Cox, P. A.; Dean, F. W. H.; Williams, A. A. *Vacuum* **1983**, *33*, 839-841.

(145) Elliott, S. D.; Bates, S. P. *Phys. Rev. B* **2002**, *65*, 245415.

(146) Elliott, S. D.; Bates, S. P. *Surf. Sci.* **2001**, *495*, 211-233.

(147) Muscat, J.; Harrison, N. M.; Thornton, G. *Phys. Rev. B* **1999**, *59*, 15457-15463.

(148) Lindan, P. J. D.; Harrison, N. M.; Gillan, M. J.; White, J. A. *Phys. Rev. B* **1997**, *55*, 15919-15927.

(149) Ng, K.-O.; Vanderbilt, D. *Phys. Rev. B* **1997**, *56*, 10544-10548.

(150) Paxton, A. T.; Thien-Nga, L. *Phys. Rev. B* **1998**, *57*, 1579-1584.

(151) Swamy, V.; Muscat, J.; Gale, J. D.; Harrison, N. M. *Surf. Sci.* **2002**, *504*, 115-124.

(152) Gillan, M. J.; Bates, S. P. *J. Phys. Chem. B* **1998**, *102*, 2017-2026.

(153) Yin, X.; Miura, R.; Endou, A.; Gunji, I.; Yamauchi, R.; Kubo, M.; Stirling, A.; Fahmi, A.; Miyamoto, A. *Appl. Surf. Sci.* **1997**, *119*, 199-202.

(154) Ramamoorthy, M.; King-Smith, R. D.; Vanderbilt, D. *Phys. Rev. B* **1994**, *49*, 7709-7715.

(155) Ramamoorthy, M.; Vanderbilt, D.; King-Smith, R. D. *Phys. Rev. B* **1994**, *49*, 16721-16727.

(156) Reinhardt, P.; Heb, B. A. *Phys. Rev. B* **1994**, *50*, 12015-12024.

(157) Grunes, L. A. *Phys. Rev. B* **1983**, *27*, 2111-2131.

(158) Lu, G.; Linsebigler, A.; Yates Jr., J. T. *J. Phys. Chem.* **1994**, *98*, 11733-11738.

(159) Lu, G.; Linsebigler, A.; Yates Jr., J. T. *J. Phys. Chem.* **1995**, *99*, 7626-7631.

(160) Lu, G.; Linsebigler, A.; Yates Jr., J. T. *J. Chem. Phys.* **1995**, *102*, 4657-4662.

(161) Epling, W. S.; Peden, C. H. F.; Henderson, M. A.; Diebold, U. *Surf. Sci.* **1998**, *412/413*, 333-343.

(162) Henderson, M. A.; Otero-Tapia, S.; Castro, M. E. *Surf. Sci.* **1999**, *114*, 313-329.

(163) Lusvardi, V. S.; Barteau, M. A.; Dolinger, W. R.; Farneth, W. E. *J. Phys. Chem.* **1996**, *100*, 18183-18191.

(164) Schaub, R.; Thostrup, P.; Lopez, N.; Laegsgaard, E.; Stensgaard, I.; Norskov, J. K.; Besenbacher, F. *Phys. Rev. Lett.* **2001**, *87*, 266104-266101-266104.

(165) Idriss, H.; Barteau, M. A. *Catal. Lett.* **1994**, *26*, 123.

(166) Lusvardi, V. S.; Barteau, M. A.; Chen, J. G.; Eng, J.; Fruhberger, B.; Teplyakov, A. *Surf. Sci.* **1998**, *397*, 237-250.

(167) Chambers, S. A.; Henderson, M. A.; Kim, Y. J.; Thevuthasan, S. *Surf. Rev. Lett.* **1998**, *5*, 381-385.

(168) Chambers, S. A.; Thevuthasan, S.; Kim, Y. J.; Herman, G. S.; Wang, Z.; Tober, E.;

Ynzunza, R.; Morais, J.; Peden, C. H. F.; Ferris, K.; Fadley, C. S. *Chem. Phys. Lett.* **1997**, *267*, 51-57.

(169) Iwasawa, Y.; Onishi, H.; Fukui, K.; Suzuki, S.; Sasaki, T. *Surf. Sci.* **1999**, *114*, 259-266.

(170) Onishi, H.; Fukui, K.; Iwasawa, Y. *Jpn. J. Appl. Phys.* **1999**, *38*, 3830-3832.

(171) Onishi, H.; Aruga, T.; Iwasawa, Y. *J. Catal.* **1994**, *146*, 557-567.

(172) Onishi, H.; Aruga, T.; Iwasawa, Y. *J. Am. Chem. Soc.* **1993**, *115*, 10460.

(173) Käckell, P.; Terakura, K. *Surf. Sci.* **2000**, *461*, 191-198.

(174) Käckell, P.; Terakura, K. *Appl. Surf. Sci.* **2000**, *166*, 370-375.

(175) Hayden, B. E.; King, A.; Newton, M. A. *J. Phys. Chem. B* **1999**, *103*, 203-208.

(176) Chang, Z.; Thornton, G. *Surf. Sci.* **2000**, *462*, 68-76.

(177) Chang, Z.; Thornton, G. *Surf. Sci.* **2000**, *459*, 303-309.

(178) Henderson, M. A. *J. Phys. Chem. B* **1997**, *101*, 221-229.

(179) Henderson, M. A.; Otero-Tapia, S.; Castrob, M. E. *Surf. Sci.* **1998**, *412/413*, 252-272.

(180) Wang, L.-Q.; Ferris, K. F.; Shultz, A. N.; Baer, D. R.; Engelhard, M. H. *Surf. Sci.* **1997**, *380*, 352-364.

(181) Onishi, H.; Sasahara, A.; Uetsuka, H.; Ishibashi, T. *Appl. Surf. Sci.* **2002**, *188*, 257-264.

(182) Onishi, H.; Yamaguchi, Y.; Fukui, K.; Iwasawa, Y. *J. Phys. Chem.* **1996**, *100*, 9582-9584.

(183) Guo, Q.; Williams, E. M. *Surf. Sci.* **1999**, *433-435*, 322-326.

(184) Idriss, H.; Legare, P.; Maire, G. *Surf. Sci.* **2002**, *515*, 413-420.

(185) Sasahara, A.; Uetsuka, H.; Onishi, H. *Surf. Sci.* **2001**, *481*, L437-L442.

(186) Wang, Q.; Madix, R. J. *Surf. Sci.* **2001**, *474*, L213-L216.

(187) Wong, G. S.; Kragten, D. D.; Vohs, J. M. *J. Phys. Chem. B* **2001**, *105*, 1366-1373.

(188) Bates, S. P.; Kresse, G.; Gillan, M. J. *Surf. Sci.* **1998**, *409*, 336-349.

(189) Ferris, K. F.; Wang, L.-Q. *J. Vac. Sci. Technol. A* **1998**, *16*, 956-960.

(190) Wang, L. Q.; Ferris, K. F.; Winokur, J. P.; Shultz, A. N.; Baer, D. R.; Engelhard, M. H. *J. Vac. Sci. Technol. A* **1998**, *16*, 3034-3040.

(191) Kieu, L.; Boyd, P.; Idriss, H. *J. Mol. Catal. A* **2002**, *188*, 153-161.

(192) Gamble, L.; Jung, L. S.; Campbell, C. T. *Surf. Sci.* **1996**, *348*, 1-16.

(193) Liu, G.; Rodriguez, J. A.; Chang, Z.; Hrbek, J. *J. Phys. Chem. B* **2002**, *106*, 9883-9891.

(194) Onishi, H.; Iwasawa, Y. *Catal. Lett.* **1996**, *38*, 89-94.

(195) Henderson, M. A. *Surf. Sci.* **1998**, *400*, 203-219.

(196) Nerlov, J.; Christensen, S. V.; Weichel, S.; Pedersen, E. H.; Moller, P. J. *Surf. Sci.* **1997**, *371*, 321-336.

(197) Hartmann, N.; Biener, J.; Madix, R. J. *Surf. Sci.* **2002**, *505*, 81-92.

(198) Sorescu, D. C.; Rusu, C. N.; Yates Jr., J. T. *J. Phys. Chem. B* **2000**, *104*, 4408-4417.

(199) Kim, S. H.; Stair, P. C.; Weitz, E. *Surf. Sci.* **2000**, *445*, 177-185.

(200) Kurtz, R. L.; Stockbauer, R.; Madey, T. E. *Surf. Sci.* **1989**, *218*, 178-200.

(201) Casarin, M.; Maccato, C.; Vittadini, A. *Appl. Surf. Sci.* **1999**, *142*, 196-199.

(202) Pan, J. M.; Maschhoff, B. L.; Diebold, U.; Madey, T. E. *J. Vac. Sci. Technol. A* **1992**, *10*, 2470-2476.

(203) Perkins, C. L.; Henderson, M. A. *J. Phys. Chem. B* **2001**, *105*, 3856-3863.

(204) Suzuki, S.; Yamaguchi, Y.; Onishi, H.; Sasaki, T.; Fukui, K.; Iwasawa, Y. *J. Chem. Soc. Faraday Trans.* **1998**, *94*, 161-166.

(205) Suzuki, S.; Yamaguchi, Y.; Onishi, H.; Fukui, K.; Sasaki, T.; Iwasawa, Y. *Catal.*

*Lett.* **1998**, *50*, 117-123.

(206) Bennett, R. A.; Newton, M. A.; Smith, R. D.; Bowker, M.; Evans, J. *Surf. Sci.* **2001**, *487*, 223-230.

(207) Evans, J.; Hayden, B. E.; Newton, M. A. *Surf. Sci.* **2000**, *462*, 169-180.

(208) Diebold, U.; Hebenstreit, W.; Leonardelli, G.; Schmid, M.; Varga, P. *Phys. Rev. Lett.* **1998**, *81*, 405-408.

(209) Hebenstreit, E. L. D.; Hebenstreit, W.; Geisler, H.; Ventrice Jr., C. A.; Hite, D. A.; Sprunger, P. T.; Diebold, U. *Surf. Sci.* **2002**, *505*, 336-348.

(210) Vogtenhunber, D.; Podloucky, R.; Redinger, J. *Surf. Sci.* **2000**, *454-456*, 369-373.

(211) Hebenstreit, E. L. D.; Hebenstreit, W.; Diebold, U. *Surf. Sci.* **2000**, *461*, 87-97.

(212) Hebenstreit, E. L. D.; Hebenstreit, W.; Geisler, H.; Ventrice Jr., C. A.; Sprunger, P. T.; Diebold, U. *Surf. Sci.* **2001**, *486*, L467-474.

(213) Firment, L. E. *Surf. Sci.* **1982**, *116*, 205-216.

(214) Mason, C. G.; Tear, S. P.; Doust, T. N.; Thornton, G. *J. Phys. Cond. Matt.* **1991**, *3*, S97-S102.

(215) Robba, D.; Ori, D. M.; Sangalli, P.; Chiarello, G.; Depero, L. E.; Parmigiani, F. *Surf. Sci.* **1997**, *380*, 311-323.

(216) Róman, E.; Bustillo, F. J.; de Segovia, J. L. *Vacuum* **1990**, *41*, 40-42.

(217) Hoflund, G. B.; Yin, H.-L.; Grogan Jr, A. L.; D.A., A.; Yoneyama, H.; Ikeda, O.; Tamura, H. *Langmuir* **1988**, *4*, 346-350.

(218) Wang, L.; Liu, J.; Cowley, J. M. *Surf. Sci.* **1994**, *302*, 141-157.

(219) Poirier, G. E.; Hance, B. K.; White, J. M. *J.Vac.Sci.Technol. B* **1992**, *10*, 6-15.

(220) Poirier, G. E.; Hance, B. K.; White, J. M. *J. Phys. Chem.* **1993**, *97*, 5965-5972.

(221) Nörenberg, H.; Dinelli, F.; Briggs, G. A. D. *Surf. Sci.* **1999**, *436*, L635-L640.

(222) Nörenberg, H.; Dinelli, F.; Briggs, G. A. D. *Surf. Sci.* **2000**, *446*, L83-L88.

(223) Fan, F.-R. F.; Bard, A. J. *J. Phys. Chem.* **1990**, *94*, 3761-3766.

(224) Watson, B. A.; Barteau, M. A. *Chem. Mater.* **1994**, *6*, 771-779.

(225) Kim, K. S.; Barteau, M. A. *Surf. Sci.* **1989**, *223*, 13-32.

(226) Idriss, H.; Pierce, K.; Barteau, M. A. *J. Am. Chem. Soc.* **1991**, *113*, 715-716.

(227) Idriss, H.; Kim, K. S.; Barteau, M. A. *Surf. Sci.* **1992**, *262*, 113-127.

(228) Idriss, H.; Libby, M.; Barteau, M. A. *Catal. Lett.* **1992**, *15*, 13-23.

(229) Idriss, H.; Kim, K. S.; Barteau, M. A. *J. Catal.* **1993**, *139*, 119-133.

(230) Kim, K. S.; Barteau, M. A. *J. Mol. Catal.* **1990**, *63*, 103-117.

(231) Pierce, K. G.; Barteau, M. A. *J. Mol. Catal.* **1994**, *94*, 389-407.

(232) Kim, K. S.; Barteau, M. A. *Langmuir* **1988**, *4*, 945-953.

(233) Barteau, M. A. *J. Vac. Sci. Technol. A* **1993**, *11*, 2162-2168.

(234) Kim, K. S.; Barteau, M. A. *J. Catal.* **1990**, *125*, 353-375.

(235) Kim, K. S.; Barteau, M. A. *Langmuir* **1990**, *6*, 1485-1488.

(236) Sherrill, A. B.; Lusvardi, V. S.; Barteau, M. A. *Langmuir* **1999**, *15*, 7615-7620.

(237) Pierce, K. G.; Barteau, M. A. *J. Phys. Chem.* **1994**, *98*, 3882-3892.

(238) Lusvardi, V. S.; Pierce, K. G.; Barteau, M. A. *J. Vac. Sci. Technol. A* **1997**, *15*, 1586-1591.

(239) Barteau, M. A. *Chem. Rev.* **1996**, *96*, 1413-1430.

(240) Kim, K. S.; Barteau, M. A.; Farneth, W. E. *Langmuir* **1988**, *4*, 533-543.

(241) Sherrill, A. B.; Medlin, J. W.; Chen, J. G.; Barteau, M. A. *Surf. Sci.* **2001**, *492*, 203-213q.

(242) Idriss, H.; Lusvardi, V. S.; Barteau, M. A. *Surf. Sci.* **1996**, *348*, 39-48.

(243) Titheridge, D. J.; Barteau, M. A.; Idriss, H. *Langmuir* **2001**, *17*, 2120-2128.

(244) Wilson, J. N.; Idriss, H. *J. Am. Chem. Soc.* **2002**, *124*, 11284-11285.

(245) Raza, H.; Pang, C. L.; Haycock, S. A.; Thornton, G. *Phys. Rev. Lett.* **1999**, *82*,

5265-5268.

(246) Landree, E.; Marks, L. D.; Zschack, P.; Gilmore, C. J. *Surf. Sci.* **1998**, *408*, 300-309.

(247) Zschack, P.; Cohen, J. B.; Chung, Y. W. *Surf. Sci.* **1992**, *1992*, 395-408.

(248) Murray, P. W.; Leibsle, F. M.; Fisher, H. J.; Flipse, C. F. J.; Muryn, C. A.; Thornton, G. *Phys. Rev. B* **1992**, *46*, 12877-12879.

(249) Murray, P. W.; Leibsle, F. M.; Muryn, C. A.; Fisher, H. J.; Flipse, C. F. J.; Thornton, G. *Phys. Rev. Lett.* **1994**, *72*, 689-692.

(250) Lo, W. J.; Chung, Y. W.; Somorjai, G. A. *Surf. Sci.* **1978**, *71*, 199-219.

(251) Henderson, M. A. *J. Phys. Chem.* **1995**, *99*, 15253-15261.

(252) Howard, A.; Motchell, C. E. J.; Morris, D.; Egdell, R. G.; Parker, S. C. *Surf. Sci.* **2000**, *448*, 131-141.

(253) Linsebigler, A.; Lu, G.; Yates Jr., J. T. *Chem. Rev.* **1995**, *95*, 735-758.

(254) Sato, S. *http://www.geocities.co.jp/Technopolis-Mars/2024/note.html, Japanese only.*

(255) Lazzeri, M.; Vittadini, A.; Selloni, A. *Phys. Rev. B* **2001**, *63*, 155409-155401-155409.

(256) Lazzeri, M.; Vittadini, A.; Selloni, A. *Phys. Rev. B* **2002**, *65*, 119901(E).

(257) Herman, G. S.; Gao, Y.; Tran, T. T.; Osterwalder, J. *Surf. Sci.* **2000**, *447*, 201-211.

(258) Herman, G. S.; Sievers, M. R.; Gao, Y. *Phys. Rev. Lett.* **2000**, *84*, 3354-3357.

(259) Liang, Y.; Gan, S.; Chambers, S. A.; Altman, E. I. *Phys. Rev. B* **2001**, *63*, 235402.

(260) Tanner, R. E.; Liang, Y.; Altman, E. I. *Surf. Sci.* **2002**, *506*, 251-271.

(261) Hebenstreit, W.; Ruzycki, N.; Herman, G. S.; Gao, Y.; Diebold, U. *Phys. Rev. B* **2000**, *62*, R16334-R16336.

(262) Hengerer, R.; Bolliger, B.; Erbudak, M.; Gra¨tzel, M. *Surf. Sci.* **2000**, *460*,

162-169.

a: $TiO_2$(110)

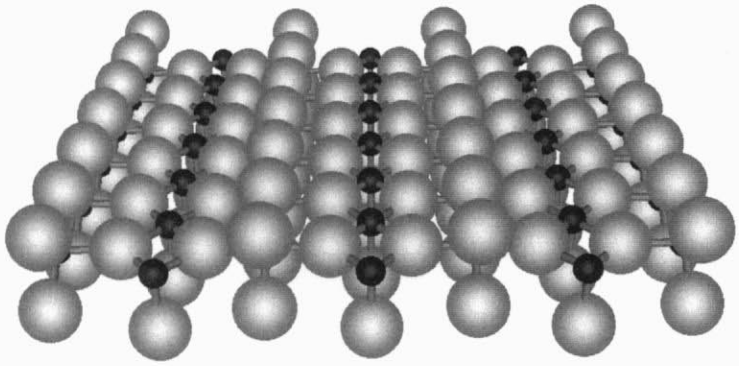

b: $TiO_2$(001)

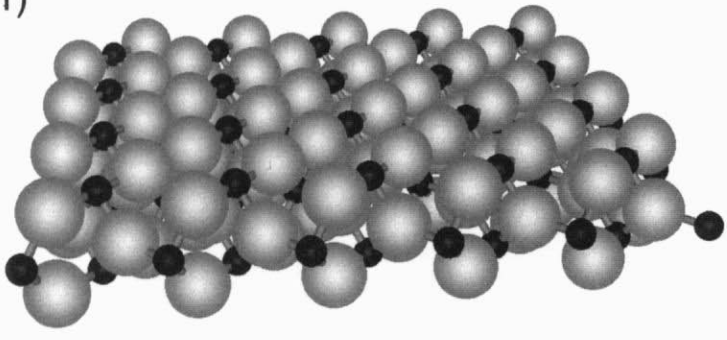

c: $TiO_2$(100)

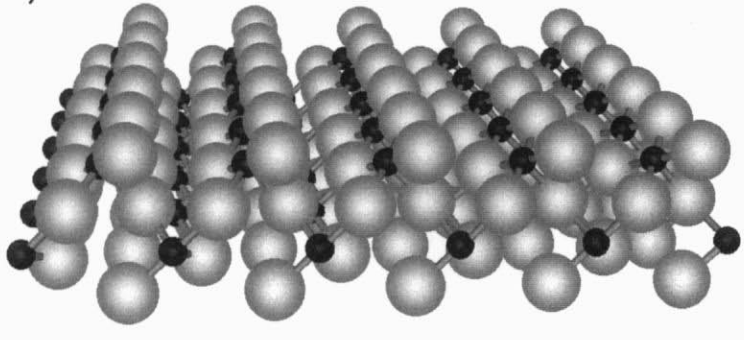

**Figure 1.1**

Bulk-terminated structural models of rutile-type $TiO_2$ single crystal. a: $TiO_2$ (110), b: $TiO_2$(001), c: $TiO_2$(100). Small black and large gray circles represent titanium and oxygen atoms, respectively.

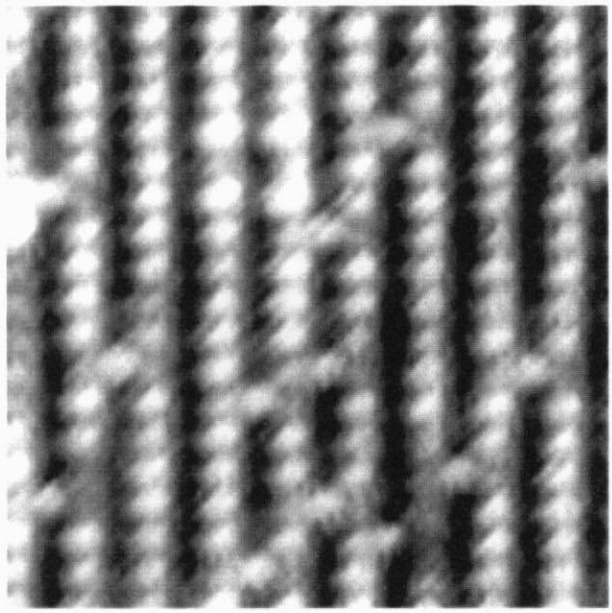

**Figure 1.2**

A constant current topograph (6.0x6.0 $nm^2$) of $TiO_2$(110)-(1x1) surface prepared by $Ar^+$-sputtering followed by annealing to 1100 K under UHV. $V_s$: 1.212 V, $I_t$: 0.15 nA.

a: $TiO_2(011)$

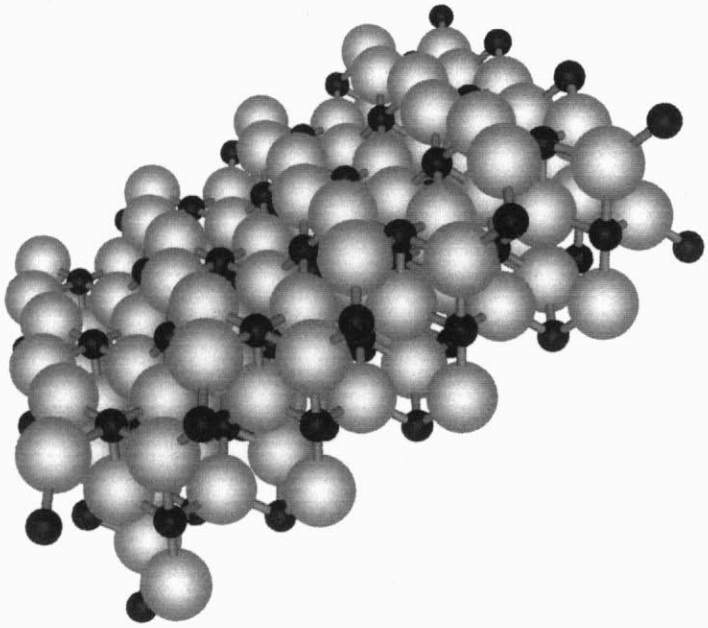

b: $TiO_2(114)$

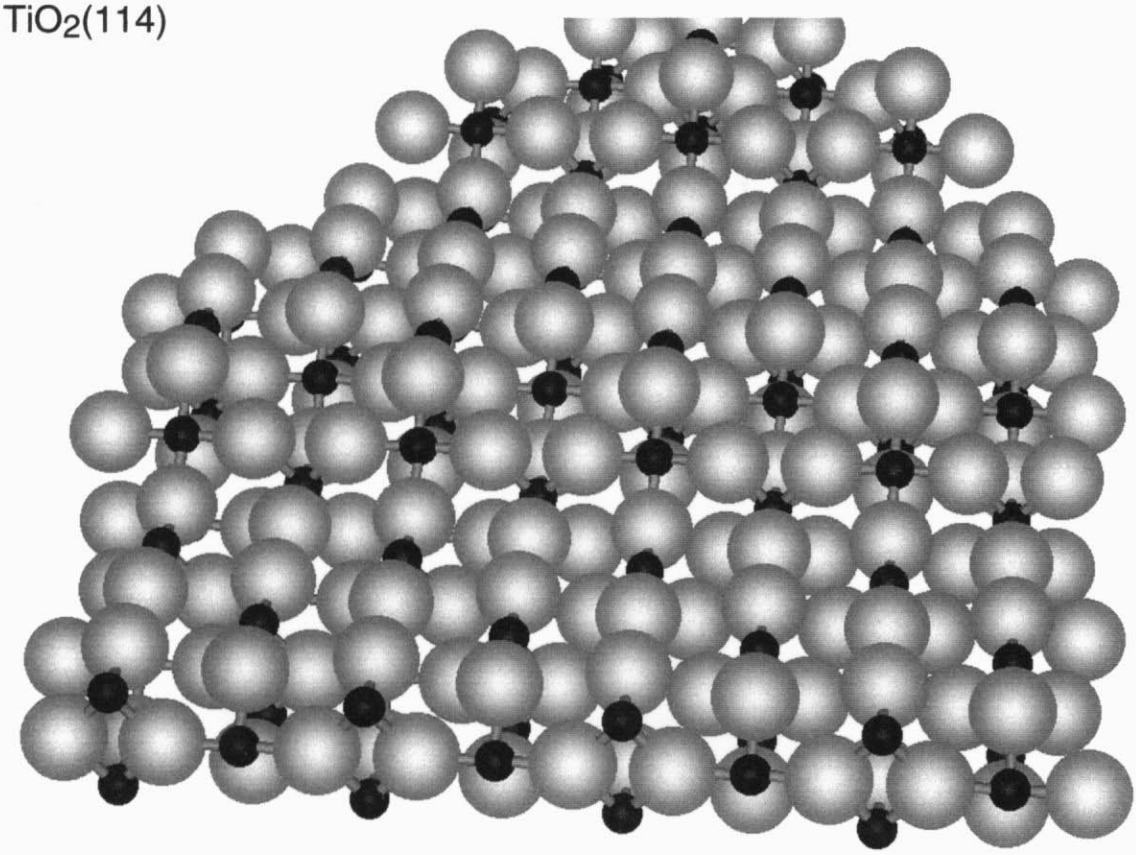

**Figure 1.3**

Bulk-terminated structures of $TiO_2$ single crystal, which has been proposed as structural models of two faceted phases on $TiO_2(001)$.
(a) $TiO_2(011)$ for lower-temperature phase, (b) $TiO_2(114)$ for higher-temperature phase.

*Chapter 2.*

# Experimental

## 2.1 Principle of Scanning Tunneling Microscopy

### 2.1.1 Outline

STM is a lensless microscopic method. The principle of STM stands on quantum mechanical tunneling and high resolution and spatial resolution less than diffraction and aberration limitations of lenses are accomplished. Figure 2.1 shows a schematic drawing of an experimental system of STM. An atomically sharp tip is held within ~1 nm from the sample surface to be studied. A bias voltage ($V_s$) is applied between the tip and sample, and quantum mechanical tunneling current ($I_t$) is measured. Any departure of $I_t$ from the settled value is corrected by negative feedback circuit loop to $z$ piezoelectric drive. Thus, when the tip is moved laterally by $xy$ piezoelectric drive remaining $I_t$ constant by feedback loop, the mapping of surface morphology can be achieved by recording the normal movement of the tip. $I_t$ is highly sensitive to the distance between tip and sample ($d$), therefore mapping with resolution of 0.01 nm in normal direction and 0.1 nm in lateral direction are possible by using an atomically sharp tip. $I_t$ decreases approximately exponentially with $d$, which corresponds to variation by about a factor of 10 for every 0.1 nm.

A STM image obtained just as mentioned above is called a "constant current topography (CCT)" (Figure 2.2a). There is another STM measurement mode called "variable current image (VCI)". In VCI mode, only average of $I_t$ is adjusted to the settled by slowing response of feedback loop, and the change of $I_t$ is recorded (Figure 2.2b). In general, VCI mode makes it possible to scan faster and acquire sharp contrast more easily than CCT mode, though no quantitative information in height is obtained in VCI mode.

It mast be noted that what is visualized in a STM image, both CCT and VCI, is a

distribution of electronic density of state. Sometimes obtained STM images are not corresponding to actual physical geometry and vary depending on $V_s$. Careful attention is necessary for interpretation of STM images.

### 2.1.2 Theory

Tunneling through a potential barrier had been already treated before development of STM to explain e.g. the characteristic of electrical current through a metal-insulator-metal (MIM). The wave functions of each electrode decay into the insulator region and overlap when the electrodes approached to in order of 1 nm. In tunneling in STM, tip and sample are considered to be each electrode and vacuum gap to be insulator. Tersoff and Hamann have given an expression for $I_t$ by first order approximation based on Bardeen's formalism[1]:

$$I_t = \frac{2\pi e}{\hbar}\sum_{\mu}^{\nu} f(E_\mu)[1 - f(E_\nu + eV_s)]\left|M_{\mu\nu}\right|^2 \delta(E_\mu - E_\nu) \ ,$$

where $f(E)$ is the Fermi function, $V_s$ is the applied voltage between tip and sample, $M_{\mu\nu}$ is the tunneling matrix element between states $\Psi_\mu$ of the tip and $\Psi_\nu$ of the surface, and $E_\mu$ and $E_\nu$ are the unperturbed energy of state $\Psi_\mu$ and $\Psi_\nu$ in the absence of tunneling.[2] The contribution of reverse tunneling is neglected and $\Psi_\mu$ and $\Psi_\nu$ are independent on the height and shape of the potential barrier between tip and sample. From the spherical-tip approximation small $V_s$ and low temperature, the equation of the local tunneling current above can lead to

$$I_t \propto \left|\Psi(R+d)\right|^2 \delta(E_\nu - E_F) \ ,$$

where $E_F$ is the Fermi energy and $R$ is the curvature radii of the sphere and $d$ is the distance between tip end and sample. Since

$$\left|\Psi(R+d)\right|^2 \propto e^{-2\kappa(R+d)} \ ,$$

where $\kappa = \sqrt{2m\phi}/\hbar$ is the minimum inverse decay length for the wave function in vacuum and $\phi$ is the work function, exponential dependence of the local tunneling current on the distance between tip and sample is indicated.

STM is also applied as spectroscopic method to investigate the surface electronic state. The method is called scanning tunneling spectroscopy (STS). The feedback loop is cut off above specific point and $I_t$ is recorded ramping $V_s$. In a first approximation it is assumed that the derivative (d $I_t$ /d $V_s$) is proportional to the local density of state of the sample. In actual experiment, calibrated value of (d $I_t$ /d $V_s$)/( $I_t$ / $V_s$) results in better agreement with density of states measured by other methods because the increase of tunneling probability with | $V_s$ | is canceled out.[3,4] In tunneling mechanism, states of the tip as well as the sample is reflected, especially in the region of $V_s < 0$.[5,6] The influence of atomic shape and electronic state of a tip on STM and STS was theoretically examined by Tsukada et al., assuming the tip various W and Pt clusters.[7]

## 2.2 Temperature Programmed Desorption

In temperature programmed desorption (TPD), a solid surface with adsorbed atoms or molecules is annealed with a constant heating rate and thermally desorbed species to gas phase against temperature is recorded by mass spectrometer. TPD is a simple but quite effective method to examine not only reaction products but also kinetics data of desorption or reaction, such as activation energy ($E_a$) and pre-exponential factor ($\nu$).

Rate of desorption ($r$) is described in Arrhenius expression, called Polanyi-Winger equation:

$$r(\theta) = -\frac{d\theta}{dt} = \nu(\theta)\theta^n e^{\left(-\frac{E_a(\theta)}{RT}\right)} ,$$

where $\theta$ represents the adsorbate coverage, $t$ the time, $\nu$ the pre-exponential factor of desorption, $n$ is the order of the desorption, $R$ the gas constant and $T$ the temperature. In the case dependency of $E_a$ and $n$ on $\theta$ is negligible, the equation is derived to

$$\ln\left(\frac{T_m^2}{\beta}\right) = \frac{E_a}{RT_m} + \ln\left(\frac{E_a}{nR\nu\theta_m^{n-1}}\right) ,$$

where $\beta = {}^{dT}/_{dt}$ represents the heating rate, $T_m$ the temperature of the peak maximum and $\theta_m$ the coverage at $T=T_m$.[8] $T_m$ is independent on $\theta$ in first-order desorption and shifts to lower in second-order desorption. In the first-order desorption, $E_a$ can be most simply estimated from $T_m$ assuming the value of $\nu$ to $10^{13}$ $s^{-1}$. Both of $E_a$ and $\nu$ can be experimentally determined from several spectra with various values of $\beta$. In order to obtain a reliable value, $\beta$ should be varied by factor of 100.

## 2.3 Apparatus

The experiments of STM and TPD were performed in two different UHV chambers.

STM images were obtained in an ultrahigh vacuum (UHV) STM (JEOL JSTM 4500VT) equipped with an $Ar^+$ ion gun (Fison) and a low electron energy diffraction (LEED)/Auger electron spectroscopy (AES) optics (OMICRON, rear-view type 4-grid SPECTRA LEED). The base pressure was $1\times10^{-8}$ Pa. A $TiO_2$ sample was mounted on an exclusive holder for JEOL JSTM. The sample holder could be inserted into the UHV chamber and settled at the required places for STM, LEED and $Ar^+$-sputtering by means of two liner transfer rods and rotatory stage. All STM images displayed in this work were

obtained at room temperature (RT) with electro-chemically etched W tips. Preparation and cleaning methods of tips were described in section 2.5. The surface temperature of the crystal was monitored by an infrared radiation thermometer.

TPD spectra were measured in another UHV chamber equipped with $Ar^+$ ion gun (VG Scientific, AG2 Sputter Ion Gun), a LEED/AES optics (VG Scientific, LEG27) and quadrapole mass spectrometer (Pfeifer, Prisma QMS200). The base pressure was $1\times10^{-8}$ Pa. The sample was mounted on a couple of electric feedthroughs for resistive heating and chrome-alumel thermocouples were attached. The temperature measured by thermocouple was calibrated to that by the infrared radiation thermometer. The heating rate during TPD measurements was 0.5-8 K $s^{-1}$.

Methanol (Wako, contamination less than detection limit), formic acid (Wako, 95 % purity) and acetic acid (Wako, 95 % purity) used in this study were purified by repeated freeze-pump-thaw cycles and introduced into the chamber through variable leak valve (ANELVA) by back-filling. The purity was checked by QMS in the chamber. Dominant impurity in formic acid and acetic acid was water. Commercial formic acid and acetic acid usually contained a few percent of because highly pure formic and acetic acids were too sensible to normally deal with. No adsorbate or product derived from water seemed detected in STM and TPD.

## 2.4 Sample Preparation

Polished $TiO_2$(001) and $TiO_2$(110) wafer were purchased from Earth Chemical Co. (Japan). The size of the wafer used in STM and TPD experiments were $6.5\times1\times0.25$ $mm^3$ and $16\times8\times1$ $mm^3$, respectively. In order to remove carbon contaminations on the surface

and defects in the bulk, the sample was annealed in air at 1073 K for 2 h before introduced into the UHV chamber. Thin Ni film was deposited on the rare side for resistive heating.

The $TiO_2$ surface was cleaned by cycles of $Ar^+$ ion sputtering (3 keV for 2 min) and annealing under UHV at 900-1100 K. Ion current of $Ar^+$-sputtering was ~1.4 $\mu$A(0.28 $\mu A/mm^2$) for $TiO_2$(110) and 0.5-1 $\mu$A(0.10-0.20 $\mu A/mm^2$) for $TiO_2$(001), which corresponded to Ar pressure of $\sim 6 \times 10^{-5}$ Pa and $\sim 2 \times 10^{-5}$ Pa in this chamber, respectively. In many cases a surface clean enough for STM observation could be obtained after only one $Ar^+$-sputtering and annealing cycle.

Special holding device was built to heat the sample linearly up to 1000 K for TPD experiments. Polished $TiO_2$ wafers with deposited Ni film on the rare side were fixed by Ta sample holder with another $TiO_2$(001) wafer without Ni film, sandwiching a small Ta foil with a spot-welded chromel-alumel thermocouple (Figure 2.3). Exposed area of the sample available for TPD was $8 \times 8$ $mm^2$. The device allowed a heating rate of at most 8 K $s^{-1}$ during TPD measurements and cleaning cycles.

## 2.5 Tip Preparation

The shape of the tip is one of the most important factors in order to obtain highly resolved STM images. Sharp tip with small cone angle and radii of curvature is ideal for reliable imaging of features on terraces and steps (figure 2.4a). Large radii of curvature of makes it impossible to resolve small features on terraces, and large cone angle leads to blurred image near steps (figure 2.4b). Sometimes overlapped images are obtained due to multi-projections at the end of the tip (figure 2.4c). It was generally called as "double tip" phenomenon. If the height of the projections on the tip was different, only protrusions on

the surface larger than the height difference between the tip projections have artifact features in the STM image. As described in following chapters, the surface structure of $TiO_2(001)$ includes so enormous number of steps that excessively strict conditions were required to obtain high-quality STM images of $TiO_2(001)$ surface comparing with $TiO_2(110)$ which consisted of large flat terraces. Chemically etched W wire has radius of curvature 10-100 nm. In order to remove contaminations and oxide layer, tip was usually cleaned before experiment. Heating by electron bombardment seems the most general way. It was also reported that focus ion beam milling leads to tip radii as small as 4 nm and cone angles of as little as 10 °.[9]

In the present study, tips were made of $\phi$0.3 mm W wires (Niraco), which were rubbed with sandpaper with mesh of 15 μm and 3 μm followed by super-sonic washing in acetone. 2 N of NaOH aqueous solutions and a platinum ring electrode were used for chemical etching. Pt ring electrode is once dipped in the NaOH solution and pulled up above the solution surface, which was then suspended by surface tension, and robe of the solution is made in the Pt ring. A short W wire held on the tip holder was settled at the center of the Pt ring electrode. Condition of the solution robe and excess length of the W wire under Pt ring are the determining factors for making a sharp tip. If the W wire is too long, excess part of the wire easily drops and torn off by the weight of itself, and the section is roughed. All tips were degassed by baking out at ~120 °C for 5-24 hours after introduced into the chamber. Further treatments are necessary to obtain satisfyingly high-resolution STM images, except for quite a few, fortunate cases.

The easiest way to sharpen a tip is additional voltage of 2-10 V to sample bias during scanning, which causes field emission accompanying with change of the shape or dropping contaminations. It can be also effective to make the tip move toward the sample and slightly touch on the step edge by increasing reference tunneling current or decreasing

sample bias. The parameters of these methods, such as value of voltage or current and its term, highly depend on one's experience. Comfortable cares must be taken, or the tip gets terrible damage impossible to recover.

In case additional voltage was ineffective or the tip was dulled by excess voltage, the tip was heated in two ways depending on the purpose. The one is irradiation from annealed Si. After the tip was settled at ~100μm form Si wafer, the Si wafer is resistively heated to 1400 K. Another way is annealing by touching the tip to red-heated W wire with its side posterior to $Ar^+$-sputtering. In the former Si-flashing-method, not only the contaminations such as carbon contained species and oxide layers are removed but also Si atoms are deposited on the tip. Therefore it is quite possible the STM images are obtained by Si mini-tip on the end of the tip. It takes an advantage to make the dull tip available, but disadvantage to specification and assignment of the observed features because apparent height and shapes of features on the surface in STM images highly depend on the tip condition. On the other hand, a clean tip is expected after $Ar^+$-sputtering followed by annealing by W wire. However this method is effective 2-3 times for each tip at most, because entire curvature of the tip end is increased after each cleaning cycle.

**References**


(1) Bardeen, J. *Phys. Rev. Lett.* **1961**, *6*, 57-59.

(2) Tersoff, J.; Hamann, D. R. *Phys. Rev. B* **1985**, *31*, 805-813.

(3) Feenstra, R. M.; Stroscio, J. A.; Fein, A. P. *Surf. Sci.* **1987**, *181*, 295-306.

(4) Lang, N. D. *Phys. Rev. B* **1986**, *34*, 5947-5950.

(5) Griffith, J. E.; Kochanski, G. P. *Crit. Rev. Solid State Mater. Sci.* **1990**, *16*, 255-289.

(6) Klitsner, T.; Becker, R. S.; Vickers, J. S. *Phys. Rev. B* **1990**, *41*, 3837-3840.

(7) Tsukada, M.; Kobayashi, K.; Isshiki, N.; Kageshima, H. *Surf. Sci. Rep.* **1991**, *13*, 265-304.

(8) Redhead, P. A. *Vacuum* **1962**, *12*, 203-211.

(9) Vasile, M. J.; Grigg, D. A.; Griffith, J. E.; Fitzgerald, E. A.; Russell, P. E. *Rev. Sci. Instrum.* **1991**, *62*, 2167.

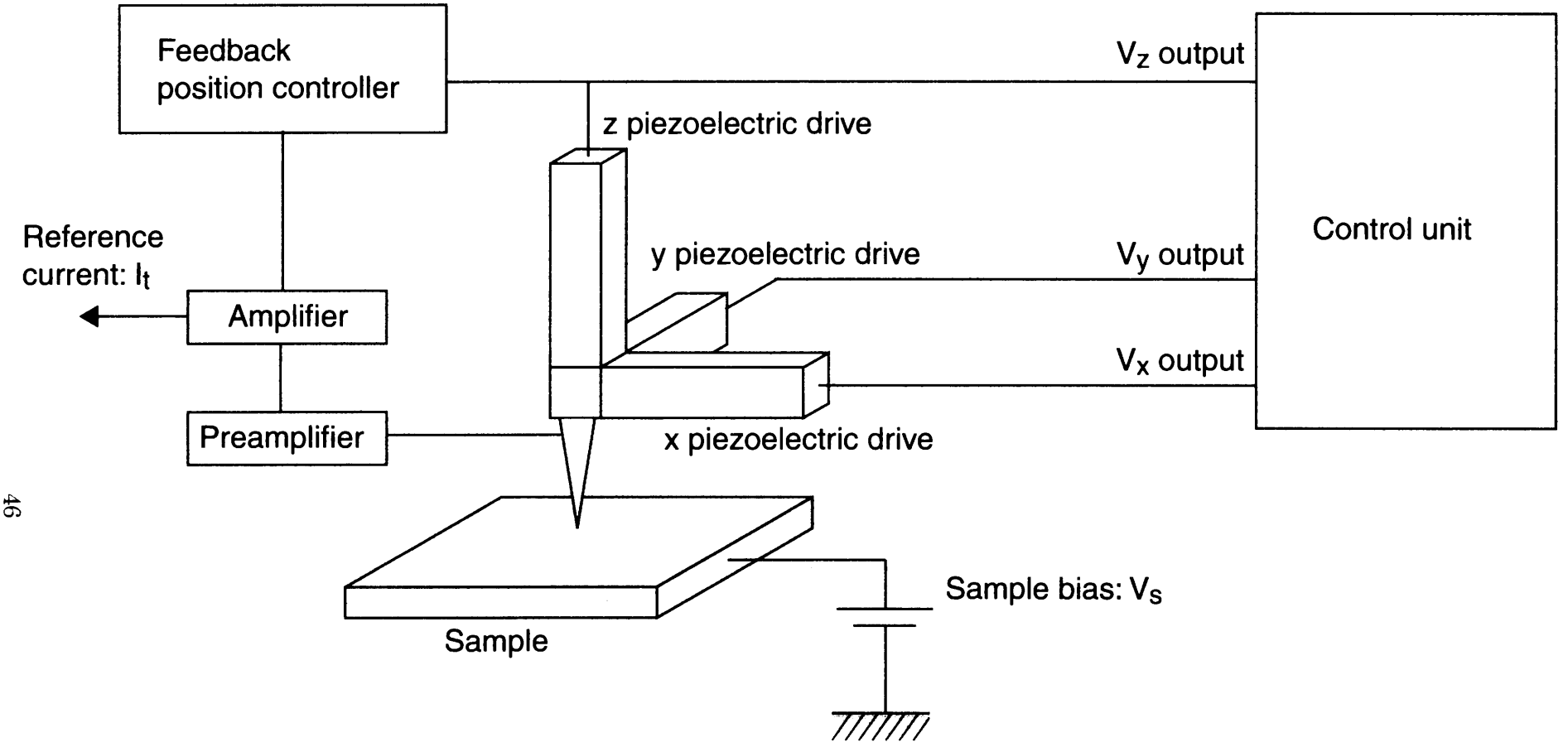


**Figure 2.1** Schematic drawing of an experimental system of STM

a. Constant Current Topograph

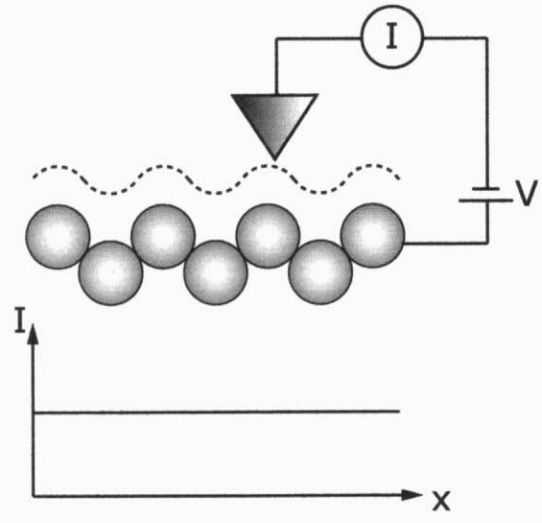


b. Variable Current Image

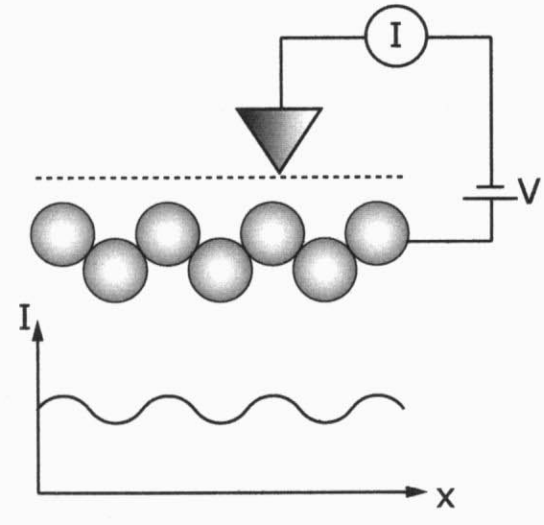


**Figure 2.2** Schematic drawings of imaging mode in STM.

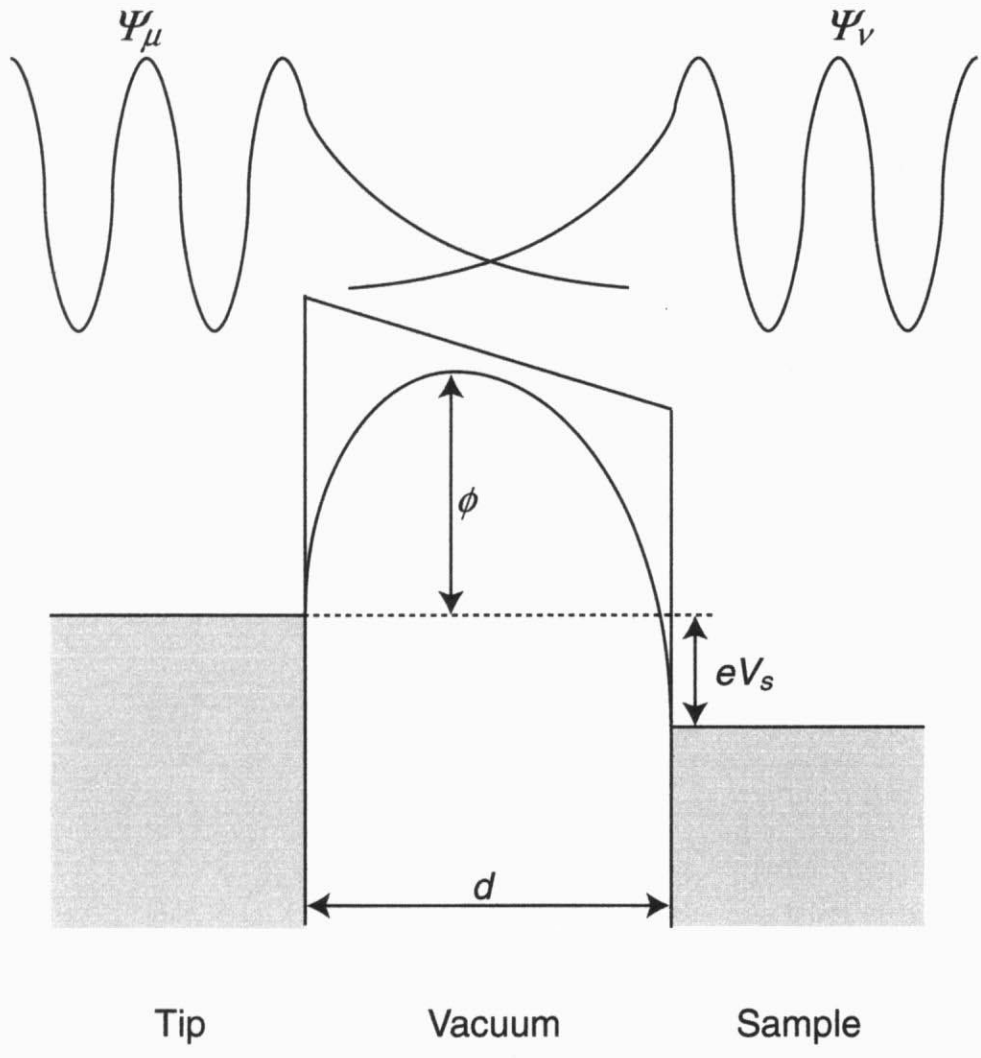


**Figure 2.3** Schematic potential diagram for STM.

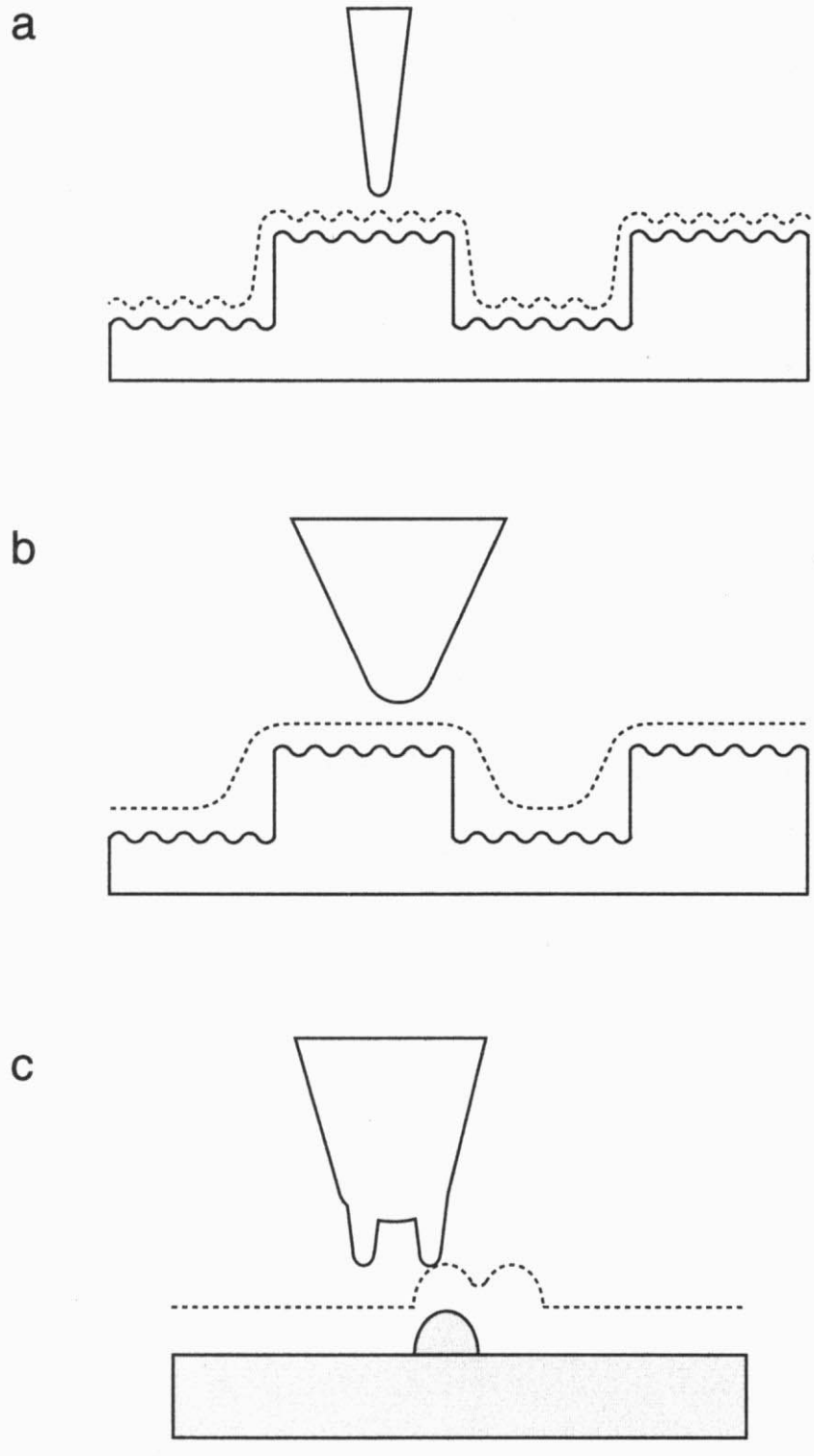


Figure 2.4 Effects of tip shape on measured STM profile.

*Chapter 3.*

# Surface Morphology of $TiO_2$(001) Investigated by Scanning Tunneling Microscopy

**Abstract**

Surface structures of a $TiO_2(001)$ surface depending on annealing temperature are examined by scanning tunneling microscopy (STM). The surface easily transformed to facet or disordered structure as previous studies. Large scale facet structure and disordered particle-like protrusions appeared after annealing the $Ar^+$-sputtered $TiO_2(001)$ at 960 K and 1160 K, respectively. However flat and atomically ordered structure was successively obtained after annealing to 1050 K by sensitively controlling cleaning conditions. The surface consisted of crossing rows along the [110] and [$1\bar{1}0$] directions. Each row had a shape of "bleachers" with stairs at both sides. The average slope was identical to the {114} plane. An atom-resolved STM image showed that each narrow terrace of the stairs was covered with a unit of three bright spots which are ordered in line perpendicular to the step and arranged with a constant separation of 0.65 nm. It was revealed that the STM image is not consistent with the previously proposed {114}-faceted model.

## 1. Introduction

Understanding of physics and chemistry of well-characterized metal oxide surfaces are of fundamental importance to develop the application of oxides to many technologies, such as catalysts, gas sensors, etc. Control and design of structures of oxide surfaces should be the forthcoming challenge to functionalize oxide surfaces.

Rutile-type $TiO_2$ is a typical transition metal oxide with various applications. The $TiO_2(110)$ surface is probably the surface whose structure has been most extensively studied by physical techniques[1] including atomic scale microscopies such as scanning tunneling microscopy (STM)[2,3] and recently developing noncontact atomic force microscopy (NC-AFM).[4] The surface structure is almost identical to the bulk-terminated one and alternating one-dimensional rows of five-fold coordinated $Ti^{4+}$ and bridging oxygen are well resolved by STM and NC-AFM, respectively. The (110) surface is the most stable surface of $TiO_2$.[1] Therefore, the surface structure remains the same during surface reaction processes monitored by STM. [5,6] In contrast, a $TiO_2(001)$ surface is believed to undergo reconstruction.[1] The bulk-terminated structure of the $TiO_2(001)$ surface is shown in Figure 3.1a. All the exposed Ti cations have four-fold coordination with oxygen anions. Therefore, the structure seems to be unstable due to extremely low coordination considering the six-fold coordination for Ti cations inside the bulk. The surface energy calculated for an unrelaxed $TiO_2(001)$ surface is twice as large as that for $TiO_2(110)$.[7] Actually, two ordered reconstructed structures depending on annealing temperature were reported by low energy electron diffraction (LEED) studies.[8,9] These two phases were assigned as two facetted structures; {011}-facets and {114}-facets , respectively, based on a kinematic LEED analysis.[9] The proposed models are schematically shown in Figure 3.1b and 3.1c, respectively. In these models, all the exposed Ti cations are converted to five-fold

coordination in Figure 3.1b, but some four-fold coordinated sites are left in Figure 3.1c. The first STM study of the surface was reported by Poirier et al..[10] They found that some preferential faceted faces grow on the surface by annealing but failed to obtain atomic-scale images. Nörenberg et al. reported atomic-scale STM images of $(7\sqrt{2}x\sqrt{2})R45°$ structure after the surface was annealed above 1300 K and subsequent quenching at a rate of ca. 100 $K\ s^{-1}$.[11] Network-like structure was observed and analyzed, however, the preparation method is quite unusual. There is no report which succeeded in obtaining atomic-scale structure of the $TiO_2(001)$ surface which was prepared with reasonable condition.

Barteau et al. have extensively studied the surface reactions on $TiO_2(001)$ by temperature-programmed reaction (TPR).[12] They found a remarkable difference in reactively between the two ordered structures. For example, carboxylic acid decomposes unimolecularly on the lower temperature phase selectively producing ketene ($H_2C=C=O$) as widely observed on other low index faces of $TiO_2$ and on other oxides.[13] On the other hand, acetone is produced as a result of bimolecular reaction of carboxylic acid on the higher temperature phase.[13] The unique activity of this surface for ketonization of carboxylates has therefore been ascribed to the four-fold coordination sites left on the surface (Figure 3.1c).

In this chapter surface morphology of $TiO_2(001)$ surface is presented. Faceted and disordered structure similar to previous studies appeared depending on annealing temperature, but I have finally succeeded in imaging the higher temperature phase of the $TiO_2(001)$ surface with atomic-scale resolution by STM. The STM images are not consistent with the previously proposed {114}-facet model (Figure 3.1c) and clearly suggests it require a new model.

## 2. Experimental

The experiments were performed in an ultrahigh vacuum (UHV) STM (JEOL JSTM 4500 VT) equipped with an $Ar^+$ ion gun and a LEED optics. The base pressure was $1 \times 10^{-8}$ Pa. A polished $TiO_2(001)$ wafer of $6.5 \times 1 \times 0.25$ $mm^3$ (Earth Chemical) was used after deposition of Ni film on the rear side of the sample to resistively heat the sample on a sample holder. The sample temperature was measured by an infrared radiation thermometer. Heating rate and cooling rate was controlled to be 7-10 K $s^{-1}$. The $TiO_2(001)$ surface was cleaned with cycles of $Ar^+$ ion sputtering (3 keV for 2 min) and annealing under UHV at ca. 900 K. STM images were obtained at room temperature (RT) with electro-chemically etched W tips.

## 3. Results and Discussion

Figure 3.2 shows STM images after annealing a $TiO_2(001)$ surface under UHV for 5 min at each determined temperature after $Ar^+$-sputtering. Starting from the rough surface after $Ar^+$-sputtering (Figure 3.2a), the surface morphology began to change after annealing ca. 900 K. This is the temperature range which used to prepare $(1 \times 1)$ structure on $TiO_2(110)$.[2] Figure 3.2b shows $TiO_2(001)$ surface after annealing to 970 K subsequent to $Ar^+$-sputtering. Large plateau structure with width of several tens of nm. Some part of the plateau had average plane of {011}. But most of the surface was disordered and simultaneous LEED showed only diffused $(1 \times 1)$ pattern. Similar plateau-like protrusions with {011} planes has been also reported in a previous STM work.[10] Figure 3.2 c shows $TiO_2(001)$ surface after annealing above 1160 K. The surface was covered with

particle-like protrusions with < 5 nm height, though LEED showed sharp subspots which can be assigned to previously reported higher-temperature phase. All particles seem to have a resemble structure, but it must be due to convolution of tip shape. These particles probably consist of substoichiometric $TiO_x$ ($x< 2$) species, because lattice oxygen begins to desorb by annealing at high temperature under vacuum. In the case of a $TiO_2(110)$ surface, double strands of $Ti_2O_3$ suboxide are added on the (1x1) structure, covering unsaturated Ti rows alternately and forming the (1x2) structure at this range of annealing temperature.[3] The different behavior between the (001) surface and the (110) surface against the annealing temperature probably reflects the different stability of surface structures. Recently, similar STM image of particle-like protrusions was reported on $TiO_2(111)$ surface after annealing around 1300 K,[14] which is also less stable than the (110) surface.

The results in Figure 3.2 show that $TiO_2(001)$ surface seems to easily transform to facet or disordered phase, as reported in the previous studies.[10,15,16] Therefore, I sensitively controlled cleaning conditions such as ion current intensity and period of $Ar^+$-sputtering, annealing temperature and a heating and cooling rate. Finally, I succeeded in constructing a flat, well-ordered structure on $TiO_2(001)$ surface. Figure 3.3 shows $TiO_2(001)$ surface annealing at 1050 K with a heating and cooling rate of 7 K $s^{-1}$, subsequent to $Ar^+$-sputtering. The surface was neither a macro-faceted nor disordered structure, but consists of rows running along the [110] direction and the [1$\bar{1}$0] direction, forming a complicated latticework. Simultaneously a sharp LEED pattern corresponding to the higher temperature phase was observed. For formation of the structure in Figure 3.3, a heating and cooling rate as well as annealing temperature was a quite important factor. The value of 7-10 K $s^{-1}$ could lead to well-ordered and homogeneous surface. I did not try to form the lower temperature phase, which had been assigned to $TiO_2(011)$-$(2\times 1)$ faceted structure.[9] The (011) plane is tilted from (001) plane by 33 degree, thus {011}-faceted structure with 20 nm width has thickness

of 13 nm at most. Penetration depth of $Ar^+$ ion beam with 2 keV energy has been estimated to 2.4 nm.[17] Therefore it can be predicted that once the surface was covered with {011}-(2×1) faceted, (011) layer could not be removed by normal cleaning process. The plateau structure in Figure3.2b is likely an initial stage of {011}-facet growth. In ref. (10), {011}-faceted structure grew after annealing at 783 K for 2 h.

Figures 3.4a and 3.4b show high resolution STM images obtained at the same area of a structure equivalent to Figure 3.3. From the constant current topograph in Figure 3.4a, it was apparent that each row running along the [110] and [1$\bar{1}$0] direction in Figure 3.3 had a shape looks like "bleachers". The slope consisted of narrow terraces and steps (Figure 3.4c). The height of each step was 0.3 nm, corresponding to single step height of $TiO_2$(001) bulk-terminated structure (Figure 3.1a). An atom-resolved variable current image (Figure 3.4b) and its magnified image (Figure3.4d) clearly shows that the bleachers-like structure is homogeneously composed of a unit cell with a size of 1.30×0.65 $nm^2$ on a projection plane parallel to the (001) surface. The units of bright spot were arranged by 0.65 nm along the [1$\bar{1}$0] direction. If the step height is taken into consideration, average slope of the bleacher-like row is the {114} plane. Therefore, it is probably the origin of the LEED pattern, which was previously assigned to {114}-facetted structure (Figure 3.1c).

Local structure of the latticework structure may be similar to that reported by Nörenberg et al..[11] After annealing a $TiO_2$(001) surface at 1773 K and quenching at a rate of 100 K $s^{-1}$, they observed by STM that rows with prismatic shape cover the surface. Although I can find some similarity on the structure of the row, the whole surface structure is quite different. As they pointed out in the paper, the structure they found is a non-equilibrium structure prepared in a quite unusual condition.[11] Therefore I do not discuss further the difference of our images and their ones. Note that I have heated and

cooled the sample with 7-10 K $s^{-1}$, which is typical rate adopted for oxide samples.

An ab initio calculation of a $TiO_2$(110)-(1x1) surface showed that a contour plot of charge densities near the conduction band minimum had maxima at undercoordinated Ti atoms in spite of physical protrusion of the bridging oxygen atoms.[18] This indicates that the undercoordinated Ti atoms have larger contribution to the tunneling current at positive sample bias voltages than the protruding oxygen atoms, i.e. exposed Ti atoms should be observed brighter than oxygen atoms. This is confirmed experimentally by adsorption of formic acid, which selectively adsorbs on exposed Ti atoms.[3] Dominant contribution of Ti atoms in STM images was also suggested by similar calculations for a $TiO_2$(110)-(1x2) added-row structure.[18] The {114}-faceted model of the $TiO_2$(001) surface consists of narrow terrace of the bulk-terminated (001) surface separated with steps of the (111) orientation (Figure 3.1c). Therefore Ti atoms exposed on the model are combination of four-fold coordinated Ti atoms with a square lattice of 0.46x0.46 nm2 on the (001) face and five-fold coordinated Ti atoms arranged in zigzag along the step edges. The minimum distance between the exposed Ti atoms along the step is 0.325 nm (Figure 3.1c). If I assume that all the exposed Ti atoms are imaged as bright spots by STM at positive sample bias voltages, the {114}-faceted model in Figure 3.1c is not consistent with the observed periodicity of bright spots with 0.65 nm along the step (Figure 3.4d). Anyway, periodicity of 0.65 nm along [110] cannot be found on the model. Although the local average slope observed in Figure 3.4 is the same as that of the {114}-faceted model, a new model is necessary to explain the observed atom-resolved image.

The driving force of surface reconstruction of $TiO_2$(001) surface is considered to be reduction in undercoordination of exposed Ti atoms, i.e. the surface cations favor to increase their coordination to oxygen anions.[1] If I compare the{114}-facetted model (Figure 3.1c) with the bulk-terminated structure (Figure 3.1a) on undercoordinated Ti atoms per lattice of

1.3 x0.65 nm2, the number of four-fold coordinated Ti atoms decreased from four to three, but two five-fold coordinated Ti atoms newly appear. Therefore, the surface is not so stabilized by the faceting. In next chapter I will examine the structure shown in Figure 3.3 and 3.4 and present a new structural model.

## 4. Summary

Surface structures of a $TiO_2(001)$ surface depending on annealing temperature after $Ar^+$ sputtering are examined in atomic-scale by STM.

1. Large plateau structure was observed after annealing at 970 K. Some part of the plateau showed included {011} plane, but the structure did not cover the whole surface. It may be possible that the plateau structure is the first stage of {011}-faceting.

2. Particle-like protrusions covered the surface after annealing above 1160 K. The particles are probably consist of $TiO_x$ ($x<2$) suboxide.

3. Flat and homogeneous latticework structure appeared after annealing at 1050 K with a heating and cooling rate of 7-10 K $s^{-1}$. The surface consisted of crossing rows along the [110] direction and the [110] direction. Each row had bleachers-like structure forming the stairs on both sides with its average slope being identical to the {114} plane. An atom-resolved STM image showed that each narrow terrace of the stairs is covered with a unit of three bright spots ordered in line perpendicular to the step and arranged with a constant separation of 0.65 nm. It was revealed that the STM image was not consistent with the previously proposed {114}-faceted model.

**References**


(1) Henrich, V. E.; Cox, P. A. *The Surface Science of Metal Oxides* ; Cambridge University Press: Cambridge, 1996.

(2) Onishi, H.; Iwasawa, Y. *Surf. Sci.* 1994 , *313* , L783-L789.

(3) Onishi, H.; Fukui, K.; Iwasawa, Y. *Bull. Chem. Soc. Jpn.* 1995 , *68* , 2447-2458.

(4) Fukui, K.; Onishi, H.; Iwasawa, Y. *Phys. Rev. Lett.* 1997 , *79* , 4202-4205.

(5) Onishi, H.; Yamaguchi, Y.; Fukui, K.; Iwasawa, Y. *J. Phys. Chem.* 1996 , *100* , 9582-9584.

(6) Iwasawa, Y.; Onishi, H.; Fukui, K.; Suzuki, S.; Sasaki, T. *Faraday Discuss.* 1999 , *114* , 259-266.

(7) Cox, P. A.; Dean, F. W. H.; Williams, A. A. *Vacuum* 1983 , *33* , 839-841.

(8) Tait, R. H.; Kasowski, R. V. *Phys. Rev. B* 1979 , *20* , 5178-5191.

(9) Firment, L. E. *Surf. Sci.* 1982 , *116* , 205-216.

(10) Poirier, G. E.; Hance, B. K.; White, J. M. *J. Vac. Sci. Technol. B* 1992 , *10* , 6-15.

(11) Nörenberg, H.; Dinelli, F.; Briggs, G. A. D. *Surf. Sci.* 1999 , *436* , L635-L640.

(12) Barteau, M. A. *Chem. Rev.* 1996 , *96* , 1413-1430.

(13) Kim, K. S.; Barteau, M. A. *J. Catal.* 1990 , *125* , 353-375.

(14) Uetsuka, H.; Sasahara, A.; Onishi, H. *Jpn. J. Appl. Phys.* 2000 , *39* , 3769-3772.

(15) Antonik, M. D.; Edwards, J. C.; Lad, R. J. *Mat. Res. Soc. Symp. Proc.* 1992 , *237* , 459-464.

(16) Watson, B. A.; Barteau, M. A. *Chem. Mater.* 1994 , *6* , 771-779.

(17) Lusvardi, V. S.; Barteau, M. A.; Chen, J. G.; Eng, J.; Fruhberger, B.; Teplyakov, A. *Surf. Sci.* 1998 , *397* , 237-250.

(18) Ng, K.-O.; Vanderbilt, D. *Phys. Rev. B* 1997 , *56* , 10544-10548.

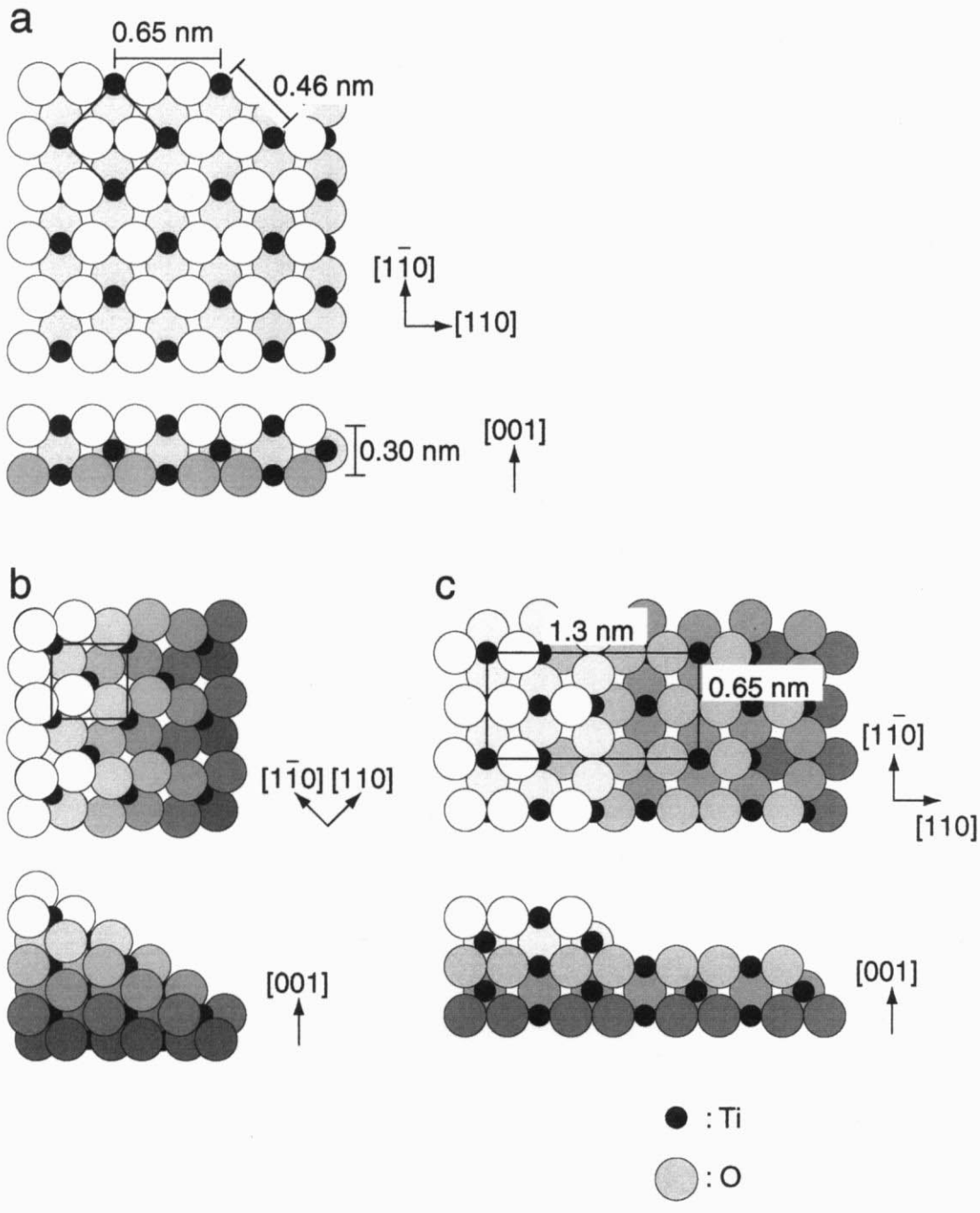


**Figure 3.1**

(a) Bulk-terminated $TiO_2$(001) surface.

(b) $TiO_2$(001)-{011}-faceted structure proposed by a LEED study (reference 9).

(c) $TiO_2$(001)-{114}-faceted structure proposed by a LEED study (reference 9).

Black solid circles and empty or shaded circles represent Ti cations and oxygen anions, respectively. Top view and side view are presented for each structure.

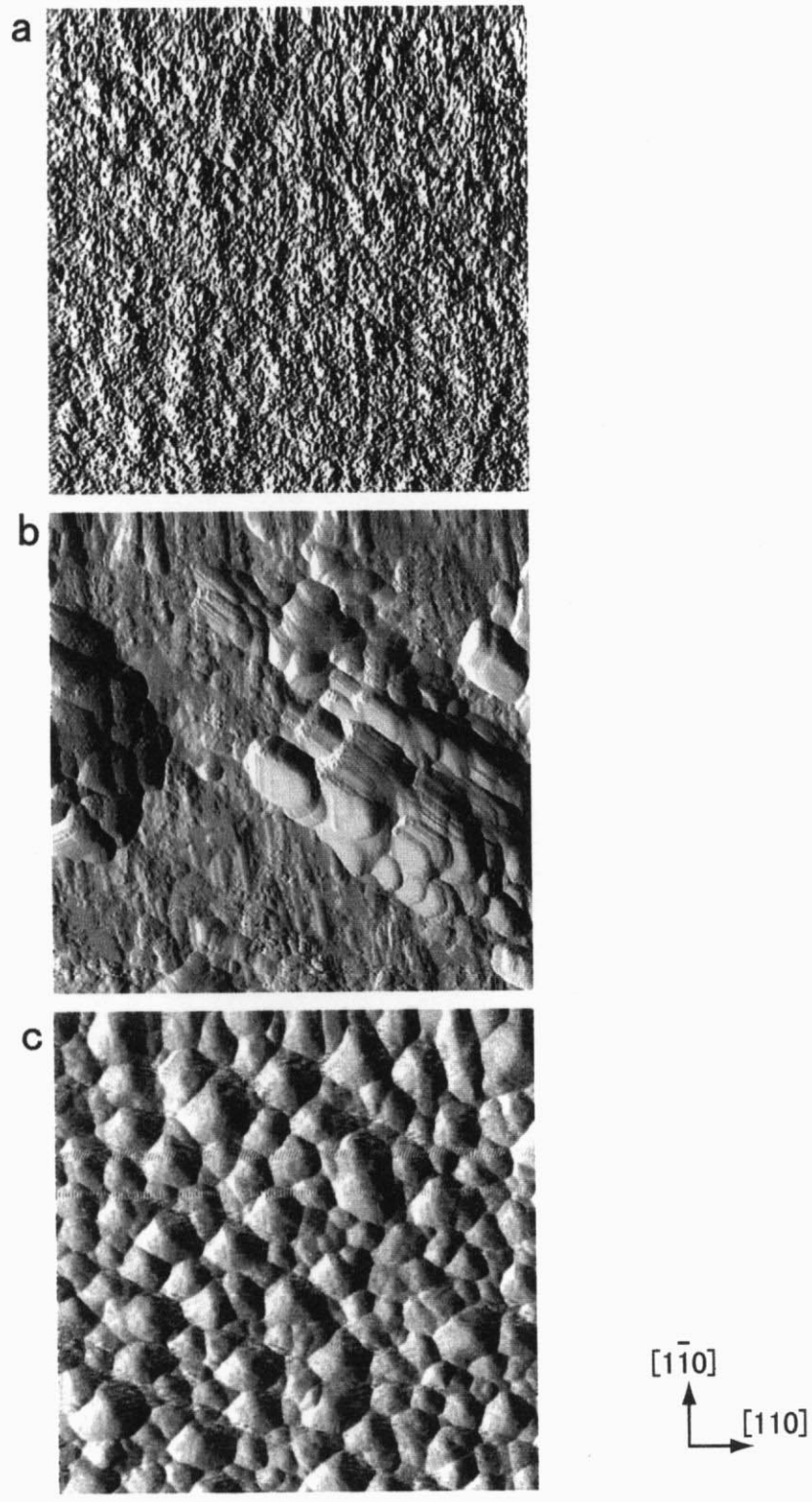


**Figure 3.2**

Varriable current images (100x100 $nm^2$) of $TiO_2$(001) surface depending on annealing temperature after $Ar^+$-sputtering. (a) Before annealing. $V_s$:+2.0 V, $I_t$: ~0.2 nA. (b) After annealing at 970 K for 5 min. $V_s$: +2.0 V, $I_t$: ~0.1 nA. (c) After annealing at 1160 K for 5 min. $V_s$: +2.0 V, $I_t$: ~0.1 nA.

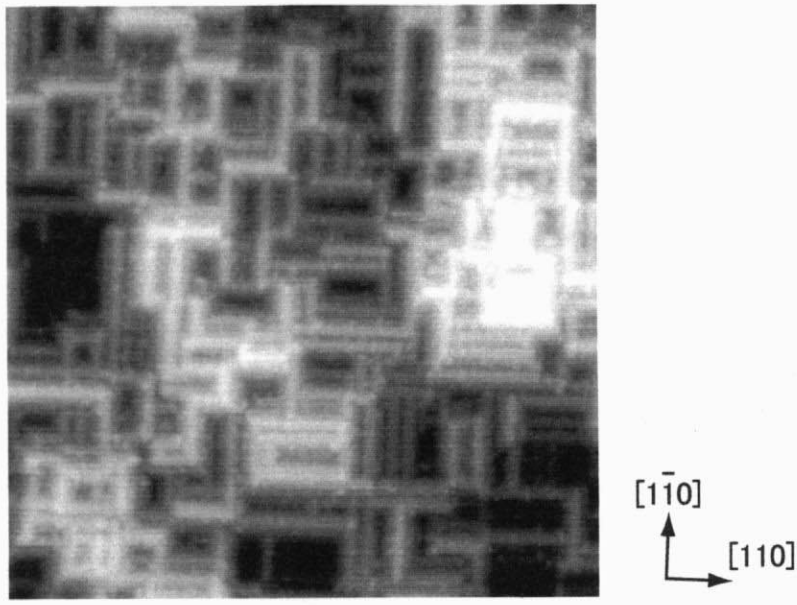


**Figure 3.3**

A constant current topograph (50.0x50.0 $nm^2$) of $TiO_2$(001) after $Ar^+$-sputtering followed by annealing at 1050 K for 5 min with a heating and cooling rate of 7 K $s^{-1}$. ($V_s$: +2.0 V, $I_t$: 0.20 nA).

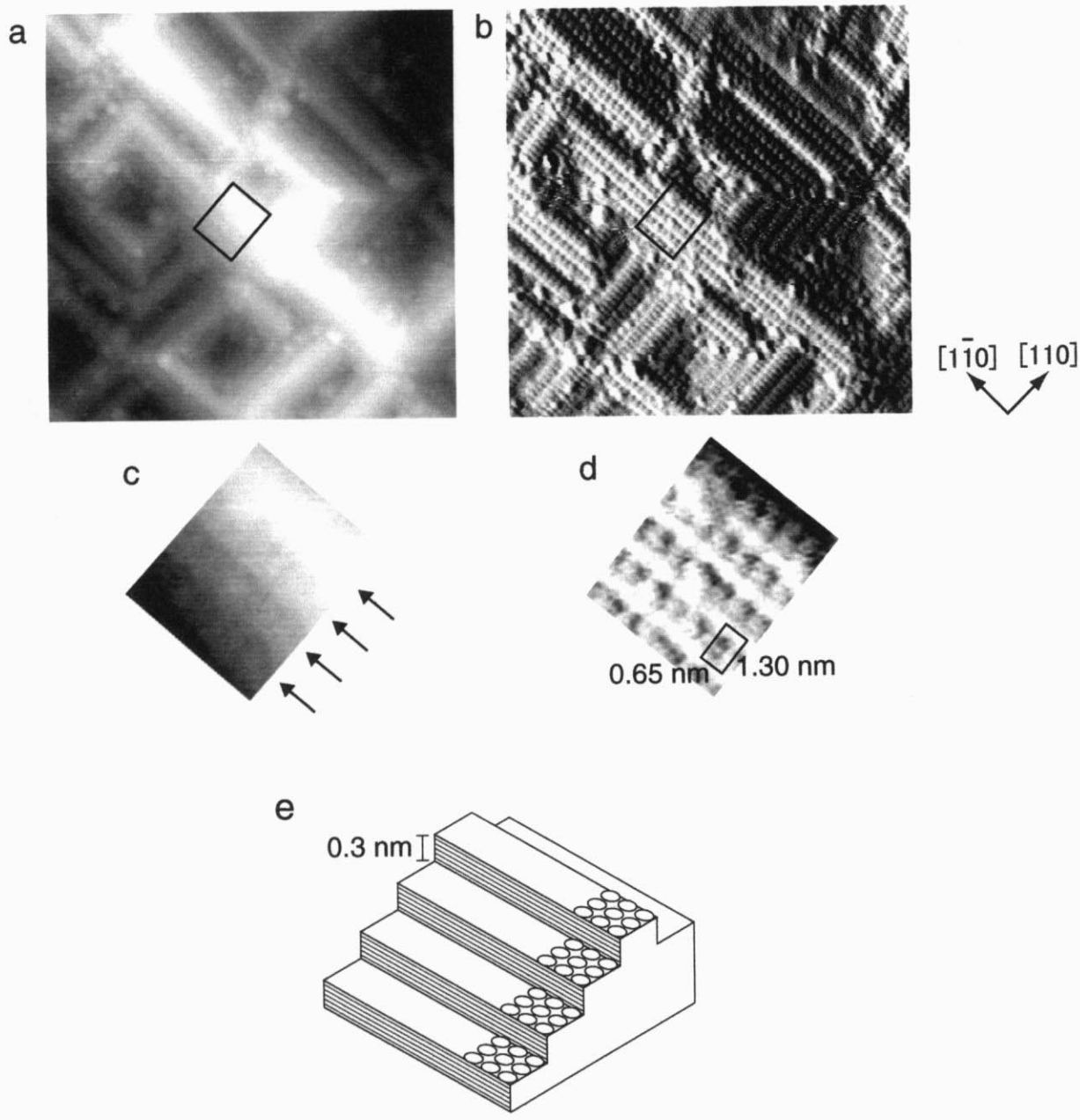


**Figure 3.4**

STM images of $TiO_2$(001) $Ar^+$-sputtered followed by annealing at 1050 K for 300 s.

(a) Constant current topograph (40.0x40.0 $nm^2$). $V_s$: +2.0 V, $I_t$: 0.10 nA.

(b) Atom-resolved variable current image (40.0x40.0 $nm^2$) obtained at the same area as (a). $V_s$: +1.6 V, $I_t$: ~0.10 nA.

(c), (d) Magnified image in the rectangular area (4.8x5.9 $nm^2$) of (a) and (b), respectively. Narrow terraces on the slope is indicated by black arrows.

(e) Schematic showing a relative relation of steps in (c) and (d).

*Chapter 4.*

# Atom-resolved Surface Structures and Molecular Adsorption on $TiO_2$(001) Investigated by Scanning Tunneling Microscopy

**Abstract**

Well-ordered surface structure was prepared on the rutile $TiO_2(001)$ surface and investigated on the atomic scale by scanning tunneling microscopy (STM). The surface had a bleachers-like structure with rows running along the [110] and $[1\bar{1}0]$ directions. Each row consisted of narrow terraces separated by single height steps on their slopes at both sides. An added-row structural model that consists of $Ti_7O_{12}$ suboxide row added on each narrow terrace of a {114}-microfacet structure was proposed based on atom-resolved STM images as well as local coordination considerations. The added row had fourfold coordinated and fivefold coordinated Ti atoms, each of which was observed as a bright spot in STM images. Formic acid molecules adsorbed on both Ti sites, while methanol adsorbed preferentially on the fourfold coordinated Ti atoms, which may support the validity of the structural model. The bleachers-like structure was proved to be stable against thermal reactions of formic acid and methanol.

## 4.1 Introduction

Metal oxides are key materials for many industrial technologies such as catalysts, gas sensors, semiconductor devices, etc.[1,2] Among a variety of oxides, the (110) surface of rutile-type $TiO_2$ has been most extensively studied as a representative oxide surface.[3,4] A $TiO_2$ (110) surface is the most stable among the low-index planes of rutile-type $TiO_2$. The surface structure of $TiO_2$(110) is almost identical to bulk termination as proved by experimental techniques[5,6] and theoretical calculations.[7,8] One-dimensional rows of fivefold coordinated Ti atoms and bridged O atoms along the [001] direction are arranged alternately. Each Ti atom and O atom in the rows has been clearly observed by scanning tunneling microscopy (STM)[4,9] and noncontact atomic force microscopy (NC-AFM),[10] respectively. Previous STM measurements of the $TiO_2$(110)-(1x1) surface during the catalytic reaction of formic acid[11,12] and the surface reaction of acetic acid[13] have shown that the surface structure is stable during the reaction. However, the surface structures have drastically changed by annealing the surface in the presence of oxygen atmosphere due to the reaction of oxygen with $Ti^{n+}$ cations that diffused to the surface from interstitial of bulk $TiO_2$, forming the added layer of $TiO_x$ (x =1-2) depending on the conditions.[14-16]

In contrast, there has been rather limited number of studies reported on $TiO_2$(001). Figure 4.1 shows a bulk-terminated structure of $TiO_2$(001) with a half-height step (0.15 nm). Cleaving between adjacent charge-neutral planes parallel to the (001) plane would produce two equivalent terraces where O-Ti-O rows are rotated by 90 degree from each other. All the exposed Ti atoms take fourfold coordination, doubly unsaturated compared with Ti atoms in the bulk. This surface is non-polar, but unstable due to low ligand coordination. Theoretical calculations have revealed that the (001) termination has significantly higher

surface energy than the (110) and the (100) termination.[7,8] Surface reconstruction was suggested to occur to stabilize the surface. In fact, two ordered phases have been observed by low energy electron diffraction (LEED) on $TiO_2$(001) depending on annealing temperature.[17,18] The lower- and the higher-temperature phases were assigned as {011}-facet and {114}-faceted structures, respectively, based on kinematic LEED analysis.[18] To date, some structural analyses of $TiO_2$(001) surfaces by scanning probe microscopies (SPM) have been reported. In the first STM observation of $TiO_2$(001), faceted structures which included mainly (011) planes were observed after annealing at 783 K for 30 min-2 h.[19] Following STM and AFM studies on $TiO_2$(001) also showed faceted or disordered reconstruction after thermal treatments under UHV.[20-22] Recently, Nörenberg et al. reported another phase of $TiO_2$(001), which appeared under non-equilibrium conditions.[23] Network-like structure with ($7\sqrt{2}$ x $\sqrt{2}$) periodicity was observed after annealing the sample to the higher temperatures than 1473 K with heating and cooling rate of 100 K/s.

Barteau and co-workers[24-27] have studied surface reactions on $TiO_2$(001) by temperature programmed desorption (TPD) for two ordered surfaces reported by the LEED study.[17,18] Chemical activity of the surfaces was extremely different among an $Ar^+$-sputtered surface, a lower-temperature phase, and a higher-temperature phase. Especially on the higher-temperature phase, which was assigned to {114}-faceted surface,[18] products of dimerization reaction were detected, such as dimethyl ether and acetone from methanol and acetic acid, respectively. These products were not detected on the lower-temperature phase as well as on the most stable $TiO_2$(110) surface. The active sites of the dimerization reactions were proposed to be fourfold coordinated Ti atoms remaining on the faceted surface. To elucidate the reason for such unique chemical activities, information of atomic-scale structure is inevitable to be obtained. However, investigation

on atomic-scale structures of ordered $TiO_2(001)$ surfaces has not been so successful, partially because it is difficult to prepare a homogeneous structure on $TiO_2(001)$, which is tolerable for precise measurements with high spatial resolution by SPM.

In this chapter, I have investigated the new structure described in chapter 3. The surface on $TiO_2(001)$ corresponded to the higher temperature phase reported by previous LEED studies. I have succeeded in imaging the surface structure on the atomic scale by STM for the first time. The surface was not a previously proposed macro-faceted structure, but an atomically ordered bleachers-like structure that consisted of stepped wide rows running along the [110] and $[1\bar{1}0]$ directions with steps and narrow terraces on their slopes. I propose a new structural model on the basis of atom-resolved STM images and adsorption of formic acid and methanol as probe molecules on the surface. The bleachers-like structure was proved to be relatively stable against reactions of adsorbed formic acid and methanol.

## 4.2 Experimental

The experiments were performed in an ultrahigh vacuum (UHV) STM (JEOL JSTM 4500VT) equipped with an $Ar^+$ ion gun and a LEED optics. The base pressure was $1x10^{-8}$ Pa. A polished $TiO_2(001)$ wafer of $6.5\times1\times0.25$ $mm^3$ (Earth Chemical) was used after deposition of Ni film on the rear side of the sample to resistively heat the sample on a sample holder. Heating rate and cooling rate was controlled to be 7-10 K $s^{-1}$. The $TiO_2(001)$ surface was cleaned with cycles of $Ar^+$ ion sputtering (3 keV for 2 min) and annealing under UHV at ca. 900 K. Constant current topographies (CCT) and variable

current images (VCI) were obtained at room temperature (RT) with electro-chemically etched W tips. Formic acid (Wako, 96 % purity, most of the contaminant is water) and methanol (Wako, contamination less than detection limit) used in this study was purified by repeated freeze- pump-thaw cycles and introduced into the chamber by back-filling. The surface temperature of the crystal was monitored by an infrared radiation thermometer.

## 4.3 Results

Figure 4.2 shows a wide range STM image (100x100 $nm^2$) after annealing an $Ar^+$-ion-sputtered $TiO_2(001)$ surface at 1050 K for 300 s with the heating and cooling rate of ca. 7 K $s^{-1}$. This surface had a bleachers-like structure that consisted of wide rows running along the [110] and [1$\bar{1}$0] directions, which were crossed and piled up. I confirmed by STM that almost the whole surface was covered with this rather flat structure by careful control of heating and cooling procedure. It was also supported from a good contrast LEED pattern simultaneously obtained from the surface (Figure 4.3). As described in chapter 3, when annealing temperature was as low as 970 K, large scale plateau structure was observed by STM as briefly reported previously. The hill-like structure was inhomogeneous on the whole surface and did not develop to flat surface at the temperature. At higher annealing temperature above 1160 K, particle-like protrusions that had wide distribution in diameter 1.5 nm-16 nm covered the surface.

The LEED pattern shown in Figure 4.3 is probably identical to that of the previously reported higher-temperature phase.[18] Annealing temperature and the primary electron energy to obtain a good contrast pattern were almost identical to the previous

studies.[18,25] Firment considered that the higher-temperature phase was faceted because the subspots did not conversed to the specular spots when the primary electron energy changed, and assigned it to a {114}-faceted structure.[18] In the present study, subspots also moved as a function of electron energy as was expected from the {114}-faceted structure, as shown in Figure 4.3. However, the corresponding surface observed by STM (Figure 4.2) was rather flat and did not seem to hold the character of typical macro-facetted structure.

Figure 4.4 shows atom-resolved STM images of the bleachers-like structure on $TiO_2$(001) shown in Figure 4.2. They included some crossing points of the rows, each of which was imaged as a wide row in Figure 4.2. Figure 4.4a clearly reveals that the each wide row consists of narrow terraces separated with steps at both sides of its slope, forming a structure like "bleachers". As shown by a magnified image at the topmost terrace of the row (Figure 4.4b), three bright spots, which were lined perpendicular to the row axis, were arranged with a regular interval of 0.65 nm along the row axis. Among the three bright spots, the center one (denoted by a filled circle) was higher than the side ones (denoted by open circles) by 0.05 nm in topography. Hereinafter we call them a "center-bright spot" and "side-bright spots", respectively. Distance between the side-bright spots and the center-bright spot was $0.50 \pm 0.04$ nm. The variable-current image in Figure 4.4c and its magnified image in Figure 4.4d show that the whole narrow terraces of the stepped wide row consist of the bright spots with the same periodicity as that of the topmost terrace. Thus, the wide row was an atomically ordered structure with a unit cell of $1.30 \times 0.65$ nm$^2$ on the projection to the (001) surface as shown in Figure 4.4d. Note that the unit cell dimension was the same as that of the {114}-faceted structure. The height difference of the narrow terraces A, B, and C in Figure 4.4a was 0.30 nm, which corresponded to the single step height of the $TiO_2$(001) surface. The average slope of the wide row was calculated to

be inclined from the (001) surface by 13 degree. Thus the average planes at both sides of the wide row corresponded to the {114} plane. The height difference between the terraces of the crossing rows (A and D or B and D in Figure 4.4a) was 0.15 nm, half of a single-step height. The structure of the wide row was equivalent regardless of the row direction. As shown in Figure 4.1, $TiO_2$(001) consists of planes with one-dimensional O-Ti-O rows, which alternately rotate by 90 degree by each other. Therefore, the bleachers-like structure holds the symmetry of the bulk-terminated $TiO_2$(001) structure.

STM observations of adsorption behavior of molecules sometimes help to characterize a surface cation sites of oxides.[28] Formic acid dissociates on $TiO_2$ surfaces to give formate anion at RT:[12]

$$HCOOH(g) + O^{2-}(s) \rightarrow HCOO^{-}(a) + OH^{-}(a) \quad (1),$$

where $O^{2-}(s)$ represents oxygen anion at the surface. Selective adsorption of formate ions on Ti cation sites has been used to identify the exposed Ti cation sites on $TiO_2$ surfaces by STM.[29] Figure 4.5a shows an STM image of the bleachers-like structure after exposure to 12 L (1 L=1.33 x $10^{-4}$ Pa s) of formic acid at RT. By comparing the image with that obtained before exposure at the same area, new bright features were observed on the narrow terraces and their density increased with exposures. Figure 4.5b is a magnified STM image of a part of a topmost terrace of a stepped wide row surrounded by a rectangle in Figure 4.5a, and Figure 4.5c is that of the same region before exposure to formic acid vapor. The newly formed bright spots had a corrugation of approximately 0.17 nm by line profile analyses along the row-axis with a small distribution. It indicates that a single adsorbate was imaged. The corrugation of the bright spot was close to that of formates (0.14 nm) on exposed Ti cations at $TiO_2$(110) with a similar tunneling condition.[29,30] Thus they can be assigned to formate ions formed by eq. (1). Although bright spots of the substrate were not resolved in

Figures 4.5b and 4.5c as in Figures 4.4, the images indicate that formate ions adsorbed on the sites expected for both center-bright spots (indicated by black arrows in Figure 4.5b) and side-bright spots (indicated by white arrows in Figure 4.5b) without any preference. Formate ions did not form any ordered structure on the surface even after further exposure. Surface hydroxyls, which were simultaneously formed with formates (eq. (1)), were not observed by STM as in the case of $TiO_2(110)$[29]. Käckell and Terakura have revealed that a surface formate on $TiO_2(110)$ surface is stabilized forming a complex with neighboring hydroxyl species.[31] It may be the reason why I could not image hydroxyl species by STM. In a recent study on formic acid adsorption on anatase $TiO_2(001)$-(1x4) surface, hydroxyl species were recognized neither by STM nor NC-AFM, although surface formate was clearly observed.[32]

Methanol is known as a much weaker Brønsted acid than formic acid. Adsorption of methanol on the bleachers-like structures was examined by STM and new bright features were observed after exposure to methanol at RT (Figure 4.6a). An apparent difference from the case of formic acid adsorption was the site of adsorbates with bright protrusions. Preferential adsorption of methanol on the center-bright spots on the narrow terraces was observed as shown in Figure 4.6b in comparison with Figure 4.6c for the image of the same area before methanol exposure. The new adsorbate was stably existed even after annealing at 400 K, by which temperature molecularly adsorbed methanol should have desorbed as reported in TPD of methanol on $TiO_2$ surface.[25,33,34] Therefore, they can be assigned to methoxy species, formed by

$$CH_3OH(g) + O^{2-}(s) \rightarrow CH_3O^-(a) + OH^-(a) \quad (2),$$

where $O^{2-}(s)$ represents oxygen anion at the surface. The methoxy species did not form ordered structure by further exposure to methanol, either. After further exposure to

methanol, however, bright spots were also observed on side-bright spots. I tentatively assign them to methoxy species migrated from the center-bright spots due to repulsive interaction between methoxy species at higher coverage. These results indicate that the center-bright spot and the side-bright spot are different not only in topographic height but also in a chemical property on adsorption of molecules.

For comparison of an adsorption property, methanol adsorption on $TiO_2$(110) surface was also examined. No features assignable to stable adsorbates were observed even after exposure to 33 L of methanol at RT (Figure 4.7). The result is quite different from that on the $TiO_2$(001) surface shown in Figure 4.6. It has been reported that majority of methanol adsorbs molecularly on $TiO_2$(110) at RT.[33,35] STM images of $TiO_2$(110)-(1x1) became blurred soon after exposure to methanol and clear images gradually recovered after continuous scanning for ~30 min. It may indicate that weakly bound methanol species were present on the surface but not imaged due to high mobility at RT.

Stability of the bleachers-like structure against thermal reaction of adsorbed molecules was examined. Figure 4.8a (4.8b) shows an STM image of the bleachers-like structure after exposure to 12 L of formic acid (48 L of methanol) at RT followed by annealing to 700 K. Previous TPD studies on the reactions of adsorbed formate and methoxy on $TiO_2$ surfaces indicated that they reacted and desorbed below 700 K.[12,24,25,33,34] Some particles were observed after formic acid reaction (Figure 4.8a). The size of the largest particle was 1.6 nm in height and 6.0 nm in diameter without correction of tip shape convolution. But it was only 3.2 % of the surface area and the bleachers-like structure was maintained in 97 % of the surface. The bleachers-like structure was entirely remained after methanol reaction (Figure 4.8b).

## 4.4 Discussion

### 4.4.1 Formation of the Bleachers-Like Structure

The bleachers-like structure observed by STM probably corresponds to the higher temperature phase in the previous studies judging from the LEED pattern, its dependency on the primary electron energy, and the similar treatment temperature.[18,25] The surface structure was homogeneous on the whole surface effective for STM measurements. I observed that the stoichiometry of the $TiO_2(001)$ substrate before annealing was important for preparing the lattice structure. Preferential sputtering of oxygen atoms and desorption of oxygen atoms during cleaning cycles gradually reduce the substrate. With a reduced substrate, the particle-like protrusions similar to Figure 3.2c formed at the lower temperature close to that used in the present study, and the control of heating and cooling rates was important to prepare the ordered bleachers-like structure. Similarly, the preparation temperature for $TiO_2(110)$-(1x2), which was slightly reduced surface phase,[29] is lowered by reduction of the substrate. Thus different degree of reduction of the substrate may be a reason why the bleachers-like structure was not observed in previous SPM studies.[19-22] In a recent STM observation of the $(7\sqrt{2} \times \sqrt{2})$ network-like structure on $TiO_2(001)$, the surface was annealed above 1473 K with heating and cooling rates of $\pm 100$ K/s.[23] I suppose the substrate would have been highly reduced on such a treatment condition. Surface periodicity from the electron diffraction pattern and the characteristics of STM images of the surface are different from the bleachers-like structure observed in the present study. Although there may be some similarity in local structure between the network structure and

the bleachers-like structure, I do not discuss the differences in detail here and concentrate on elucidating the atomic-scale surface structure of the stepped wide rows.

### 4.4.2 Atomic-Scale Structure of the Bleachers-Like Structure

Constant current topography measurements are affected not only by physical geometry but also by local electronic density of states of the tip and the sample. At a positive sample bias voltage ($V_s$) that I used for stable surface imaging of $TiO_2$(001) surfaces, the major path for tunneling electrons is from the Fermi energy of the tip to the unoccupied states of sample surface (the Fermi energy of the sample + $eV_s$).[36] Rutile $TiO_2$ bulk has a filled valence band of predominantly O 2p character and an empty conduction band of predominantly Ti 3d character, separated by a band gap of 3.1 eV.[1] The $TiO_2$(110) surface consists of alternating rows of fivefold coordinated Ti rows at the troughs and bridging O rows at the ridges, which locate 0.11 nm above the underlying Ti-O plane. It has been established from an *ab initio* calculation that fivefold coordinated Ti atoms are observed higher than the bridging oxygen atoms in constant current topography at positive sample bias voltages.[37] STM observation of selective adsorption of formic acid on fivefold Ti sites also supported the conclusion.[29,30] Thus preferential tunneling to unoccupied states with Ti 3d character overcomes the physical geometry. On $WO_3$(001) surface, which is also a $d^0$ metal oxide, it has been reported that physical geometry remained in STM images: on-top oxygen atoms were visible as bright spots even at positive sample bias voltages because significant mixing of W 5d state with O 2p state increased the unoccupied density of states at oxygen atoms.[38,39]

Formic acid dissociatively adsorbs on Ti cations of $TiO_2$ surfaces to form a

formate ion at room temperature by eq. (1). Thus this molecule has played a crucial role as a probe to identify exposed Ti sites on $TiO_2$(110) by STM.[29,30] It is now established from experiments[29,30,40-42] and a theoretical calculation[31] that formate ions adsorb with a bridged configuration through two oxygen atoms of formate to two fivefold coordinated Ti atoms with a 0.3 nm separation on $TiO_2$(110)-(1x1). Atom-resolved STM observations (Figure 4.4) revealed that the bleachers-like structure consisted of narrow terraces separated by steps and each narrow terrace was covered with ordered bright spots as schematically shown in Figure 4.4d. Formate ions adsorbed on the sites corresponding to the bright spots of the substrate (Figure 4.5b). Therefore I consider that the bright spots of the substrate can be assigned to coordinatively unsaturated Ti atoms. The bright protrusion of a formate ion observed by STM is probably due to electron tunneling to the lowest unoccupied molecular orbital (LUMO) localized at O-C-O.[30] Although it is difficult to determine the adsorption configuration by STM, formate ions on the bleachers-like structure probably adsorb as unidentate or bidentate forms because the distance between two neighboring center-bright spots and between the center-bright spot and the side-bright spot, 0.65 nm and 0.50 nm, respectively, is too far from each other for a formate to form a bridge configuration.

The upper left side of Figure 4.9 shows a bulk-terminated {114}-faceted structure, which was previously proposed for the structure for the higher-temperature phase. Note that a combination of {114}-microfacet with several step-depths can reproduce the gross feature of the STM image in Figure 4.4, where row structures with narrow terraces separated by single height steps are running along the [110] and the [$1\bar{1}0$] directions. However, the {114}-microfaceted model cannot reproduce the details of the atom-resolved STM image. In a unit cell surrounded by a rectangle, which is equivalent to that in Figure 4.4d, five Ti atoms are exposed: three fourfold coordinated Ti atoms on the terrace and two fivefold

coordinated Ti atoms on the zigzag steps. Positions of the exposed Ti atoms in the unit cell are drawn at the top left of Figure 4.9. They are not consistent with the positions of the bright spots in Figure 4.4. In addition, if I compare the {114}-microfaceted model with a flat $TiO_2$(001) bulk-terminated surface, the density of fourfold coordinated Ti atoms is lower but the total coordination number of exposed Ti atoms to O atoms per a unit cell is the same (Table 4.1). Therefore significant stabilization cannot be expected for the {114}-faceted model. Although large displacements of atom positions to reduce high surface energy of a bulk truncated $TiO_2$(001) surface have been suggested by several theoretical calculations,[7,8,43,44] there is a distinct limitation in predict ion of the surface structure, which may be different from bulk-truncated one in composition, by *ab initio* calculation at present. These results indicate that the atom-resolved STM images obtained here is a clue to construct a new structural model.

$TiO_2$ is a $d^0$ metal oxide and Ti cations hold the highest oxidation states. In reduced form, $Ti_2O$, TiO, $Ti_2O_3$, $Ti_3O_5$ are well known as separate compounds. Besides these compounds, two series of Magnéli phase exist between $TiO_2$ and $Ti_3O_5$. Magnéli phases consist of slabs of the rutile structure separated by a regular array of crystallographic shear (CS) planes, in which certain lattice planes move relative to each other as a result of planar defect clustering leading to the collapse of the lattice. The {121} series with $Ti_nO_{2n-1}$ ($4<n<10$) and the {132} series with $Ti_nO_{2n-1}$ ($16<n<\sim37$) are formed and some of the CS planes appeared on $TiO_2$(110) have been analyzed by STM.[45-47] Local structures of the compounds were examined if they fit to the narrow terrace of the bleachers-like structure, but it failed. Although the {112} series CS planes[47] may form narrow terraces separated by single height steps along the [110] and [1$\bar{1}$0] directions, the average plane of the slope is different from the bleachers-like structure ({114} planes) and the shear process dose not

change the structure of each terrace from the bulk-terminated one.

At ternary oxide systems of Ti with Cr, Ga, Fe etc., it has been pointed out that Ti cations diffuse into empty octahedral void of oxygen anions at the first stage of the formation of CS planes.[48,49] I have previously proposed on the basis of STM observations that $Ti_2O_3$ added row was formed on slightly reduced $TiO_2$(110)-(1x1) as a surface-limited phase.[9,14,29,50] In the $Ti_2O_3$ added row model, $Ti^{3+}$ are positioned at interstitial octahedral sites of oxygen atoms whose positions are assumed to be an extension of the substrate bulk. The model has been supported by the results of ESDIAD,[51] NC-AFM,[10,52] and a theoretical calculation.[53] I constructed a structural model for the bleachers-like structure following the concept of $Ti_2O_3$ added row on $TiO_2$(110). I added a suboxide row on each narrow terrace of the {114}- microfaceted structure.

I constructed a model to reproduce the atom-resolved STM image in Figure 3 on the basis of several assumptions as follows;

1) one exposed Ti atom corresponds to one bright spot in the STM image as discussed above,

2) oxygen atoms are located at bulk-extended positions of the substrate and Ti atoms are located within reasonable distances from oxygen atoms (0.179-0.186 nm for $Ti_2O_3$ added row[53] and 0.194-0.197 nm for $TiO_2$ bulk) with preference to bulk-extended positions or interstitial positions of octahedral oxygen void,

3) total coordination number of exposed Ti cations (five is the maximum for each exposed Ti cation) in a unit cell is as large as possible for surface stabilization,

4) O/Ti ratio is equal to or less than 2, because the surface is somewhat reduced after annealing to 1050 K under UHV.

A model of added-row structure is shown in Figure 4.9. A suboxide row, which contains

four interstitial $Ti^{3+}$ (=$Ti_4O_6$) and three exposed $Ti^{4+}$ (=$Ti_3O_6$) per the unit cell, is added on narrow terraces of the {114}-microfaceted structure. Stoichiometry of the added suboxide-row is $Ti_7O_{12}$ (=$TiO_{1.71}$) at the top terrace and $Ti_7O_{11}$ (=$TiO_{1.57}$) at other narrow terraces on the {114}-slopes of the stepped wide row. It should be noted that all the atoms in the added-row model hold bulk-extended positions except for the interstitial Ti atoms. Thus the intersection of crossing rows observed in Figure 4.4 can be easily reproduced as shown in the lefthand side of Figure 4.9. Positions of the exposed Ti atoms in the added-row model are schematically illustrated at the top right of Figure 4.9. I can safely assume that three exposed Ti atoms represented by black dots mainly contribute to electron tunneling at the top terrace due to a geometric reason. Therefore the center-bright spots and the side-bright spots observed in Figure 4.4 probably correspond to fourfold coordinated Ti atoms at the center of the row and fivefold coordinated Ti atoms at both sides, respectively. The fivefold coordinated Ti atoms that face to step edges on lower terraces are difficult to be resolved in STM images due to a finite radius tip apex. Thus, at narrow terraces on the slope of the stepped wide row, it is expected that two of the three exposed Ti atoms in the unit cell are mainly resolved by STM. These are consistent with the STM images shown in Figure 4.4. As shown in Table 4.1, the total number of unsaturated ligand coordination of exposed Ti atoms as well as the number of fourfold coordinated Ti atoms per a unit cell are lower than those of the bulk-terminated $TiO_2$(001) and the bulk-terminated {114}-faceted model.

Formate ions adsorbed on the stepped wide row are schematically drawn at lower part of Figure 4.9, tentatively assuming bidentate form for a center-bright spot (fourfold coordinated Ti) and unidentate form for a side-bright spot (fivefold coordinated Ti). It should be noted, however, that I could not observe formate ions at sites on the side-bright

spots that face to step edges on the lower terrace. At the step between the topmost terrace and the second terrace in Figure 4.9, local geometry of fivefold coordinated Ti atoms of the added row on the second terrace and fivefold coordinated Ti atoms of the bulk-terminated structure are almost the same. If a formate ion is placed on these sites in a unidentate or bidentate form, the {111}-slope of the added-row facing across the trough is close to overlap the van der Waals spheres of O atoms or a C atom of the formate ion. Thus, adsorption of formic acid on these sites seems to be difficult due to steric blocking even if these Ti atoms are coordinatively unsaturated.

Although the periodicity of the added row model along the row axis (0.65 nm) coincides with STM images, the distance between a fourfold coordinated Ti atom and a neighboring fivefold coordinated Ti atom (0.325 nm) is smaller than the observed value (~0.5 nm). Height difference between the fourfold coordinated Ti atom and the neighboring fivefold coordinated Ti atom in the model is 0.15 nm, which is slightly larger than the observed value of 0.05 nm (Figure 4.4b). As noted above the bulk-extended positions are assumed for most of the atoms in the added row model. The observed structure may be somewhat relaxed from the model perpendicular to the row axis due to the presence of interstitial Ti atoms. Such relaxation makes the discrepancies smaller, but I did not dare to relax the model without any substantial information. Besides, the difference in the direction parallel to the surface may be explained by the direction of an orbital extended from the unsaturated Ti atoms. On a Si(111)-(3x2) reconstructed surface, characteristic pentagonal group of spots has been observed in STM images at a positive sample bias voltage and were assigned to dangling bond states of five-membered Si rings.[53-56] A theoretical calculation on its optimum surface structure and STM image expected from the structure revealed that pentagonal bright spots in the STM image deviated outside of the

five-membered Si ring by 0.08-0.18 nm due to tilt of the dangling bonds from the surface normal. In the case of the present study, an empty state lobe of the fivefold coordinated Ti atom on the added row can be expected to extend normal to the slope of the added row. Therefore it may be possible that the tilted empty state lobe at the fivefold coordinated Ti atom in the added row caused bright spots at larger separation from the fourfold coordinated Ti atom than the geometric separation in the model.

Methanol adsorption on the bleachers-like structure indicated that the center-bright spot (fourfold coordinated Ti atom in Figure 4.9) and the side-bright spot (fivefold coordinated Ti atom in Figure 4.9) differ not only in topographic height but also in a chemical property on dissociative adsorption of methanol. Methanol preferentially adsorbed on the fourfold coordinated Ti atoms as methoxy species (Figure 4.6). Dissociative adsorption process of eq. (2) involves two substrate atoms (Ti and O). A surface oxygen atom withdraws proton from $CH_3OH$ to form surface hydroxyl. It suggests that local geometry and electronic states of a neighboring O atom are also important for the process. However, there is always neighboring oxygen atoms with similar unsaturated coordination and similar distance for both kinds of Ti atoms. Therefore I consider that the difference in chemical property can be attributed to the difference in coordination number of Ti cation. On $TiO_2$(110) surface, which contains only fivefold coordinated Ti atoms, majority of methanol adsorbed molecularly at RT.[33,35] Our STM measurements on $TiO_2$(110) supported this view.

The added-row model in Figure 4.9 seems to be an appropriate model that is consistent with the atom-resolved STM images of the surface and molecule-adsorbed STM images. It also has a reasonable stoichiometry and local coordination around each atom. For further elucidation of the structures, NC-AFM measurements for protruding oxygen

atoms, which cannot be observed by STM,[10] medium energy ion scattering spectroscopy, and theoretical calculations with a rather large system would be helpful.

### 4.4.3 Bleachers-Like Structure as a Reaction Field

Stability of a surface structure against adsorption and reaction of adsorbed molecules is an important issue particularly for catalytic reactions on the surface. Neither large displacement of atoms nor reconstruction of the bleachers-like structure on $TiO_2(001)$ were observed after the adsorption of formic acid and methanol as shown in Figure 4.5 and Figure 4.6. Particularly for methanol no structural change was observed even after repeated cycles of adsorption and reaction by annealing to 700 K (surface after a cycle is shown in Figure 4.8b). In the case of formic acid, some protrusions with unknown composition were formed after the thermal reaction (Figure 4.8a), though the density of the protrusions was small enough. Repeated cycles of adsorption and reaction increased the density of such protrusions. Precise analyses of reaction products are necessary to discuss the details, but I assume that a change in local stoichiometry caused formation of such protrusions. Addition of oxygen atoms from formate to the added row may lead to reaction with Ti cations diffused from bulk interstitials to the surface. Actually, formation of $TiO_x$ by oxidation of such Ti cations has been confirmed by STM.[14-16] Except for such minor reaction, stability of the bleachers-like structure on $TiO_2(001)$ is rather high in contrast to the bulk-terminated structure. It can be expected that this surface works as an effective reaction field in a catalytic reaction system as partly shown in effective adsorption ability of methanol as methoxy species.

## 4.5 Summary

Surface structure of the rutile $TiO_2(001)$ was examined by STM on the atomic scale. After annealing to 1050 K under ultrahigh vacuum subsequent to $Ar^+$-sputtering, the bleachers-like structure that consisted of atomically ordered stepped wide rows like "bleachers" running along the [110] and $[1\bar{1}0]$ directions were observed. This surface was assigned to the higher temperature phase reported in previous LEED studies. Based on atom-resolved STM images as well as local coordination considerations, I proposed an added-row structural model, which consists of $Ti_7O_{12}$ suboxide row added on each narrow terrace of a {114}-microfacet structure. The added row contained fourfold coordinated and fivefold coordinated Ti atoms, each of which was observed as bright spot in the STM images and formic acid adsorbed on each site. Preferential adsorption of methanol on the specific sites supported the assignment of the two kinds of exposed Ti.

**References**


(1) Henrich, V. E.; Cox, P. A. *The Surface Science of Metal Oxides*; Cambridge University Press: Cambridge, 1996.

(2) Iwasawa, Y. *Stud. Surf. Sci. Catal.* **1996**, *101*, 21.

(3) Lai, X.; Clair, T. P. S.; Valden, M.; Goodman, D. W. *Prog. Surf. Sci.* **1998**, *59*, 25.

(4) Diebold, U. In *Chem. Phys. Solid Surf.*; King, D. A., Woodruff, D. P., Eds.; Elsevier: Amsterdam, 2001; Vol. 9, pp 443.

(5) Maschhoff, B. L.; Pan, J. M.; Madey, T. E. *Surf. Sci.* **1991**, *259*, 190.

(6) Charlton, G.; Howes, P. B.; Nicklin, C. L.; Steadman, P.; Taylor, J. S. G.; Muryn, C. A.; Harte, S. P.; Mercer, J.; McGrath, R.; Norman, D.; Turner, T. S.; Thornton, G. *Phys. Rev. Lett.* **1997**, *78*, 495.

(7) Ramamoorthy, M.; Vanderbilt, D.; King-Smith, R. D. *Phys. Rev. B* **1994**, *49*, 16721.

(8) Muscat, J.; Harrison, N. M. *Surf. Sci.* **2000**, *446*, 119.

(9) Onishi, H.; Iwasawa, Y. *Surf. Sci.* **1994**, *313*, L783.

(10) Fukui, K.; Onishi, H.; Iwasawa, Y. *Phys. Rev. Lett.* **1997**, *79*, 4202.

(11) Iwasawa, Y.; Onishi, H.; Fukui, K. *Topics in Catal.* **2001**, *14*, 163.

(12) Onishi, H.; Aruga, T.; Iwasawa, Y. *J. Catal.* **1994**, *146*, 557.

(13) Onishi, H.; Yamaguchi, Y.; Fukui, K.; Iwasawa, Y. *J. Phys. Chem.* **1996**, *100*, 9582.

(14) Onishi, H.; Iwasawa, Y. *Phys. Rev. Lett.* **1996**, *76*, 791.

(15) Bennett, R. A.; Stone, P.; Price, N. J.; Bowker, M. *Phys. Rev. Lett.* **1999**, *82*, 3831.

(16) Li, M.; Hebenstreit, W.; Gross, L.; Diebold, U.; Henderson, M. A.; Jennison, D. R.; Schultz, P. A.; Sears, M. P. *Surf. Sci.* **1999**, *437*, 173.

(17) Tait, R. H.; Kasowski, R. V. *Phys. Rev. B* **1979**, *20*, 5178.

(18) Firment, L. E. *Surf. Sci.* **1982**, *116*, 205.

(19) Poirier, G. E.; Hance, B. K.; White, J. M. *J. Vac. Sci. Technol. B* **1992**, *10*, 6.

(20) Watson, B. A.; Barteau, M. A. *Chem. Mater.* **1994**, *6*, 771.

(21) Nörenberg, H.; Dinelli, F.; Briggs, G. A. D. *Surf. Sci.* **2000**, *446*, L83.

(22) Antonik, M. D.; Edwards, J. C.; Lad, R. J. *Mat. Res. Soc. Symp. Proc.* **1992**, *237*, 459.

(23) Nörenberg, H.; Dinelli, F.; Briggs, G. A. D. *Surf. Sci.* **1999**, *436*, L635.

(24) Kim, K. S.; Barteau, M. A. *Langmuir* **1990**, *6*, 1485.

(25) Kim, K. S.; Barteau, M. A. *Surf. Sci.* **1989**, *223*, 13.

(26) Kim, K. S.; Barteau, M. A. *J. Catal.* **1990**, *125*, 353.

(27) Barteau, M. A. *Chem. Rev.* **1996**, *96*, 1413.

(28) Iwasawa, Y. *Surf. Sci.* **1998**, *404-404*, 8.

(29) Onishi, H.; Fukui, K.; Iwasawa, Y. *Bull. Chem. Soc. Jpn.* **1995**, *68*, 2447.

(30) Onishi, H.; Iwasawa, Y. *Chem. Phys. Lett.* **1994**, *226*, 111.

(31) Käckell, P.; Terakura, K. *Surf. Sci.* **2000**, *461*, 191.

(32) Tanner, R. E.; Sasahara, A.; Liang, Y.; Altman, E. I.; Onishi, H. *J. Phys. Chem. B* **2002**, *106*, 8211.

(33) Henderson, M. A.; Otero-Tapia, S.; Castro, M. E. *Faraday Discuss.* **1999**, *114*, 313.

(34) Róman, E.; Bustillo, F. J.; de Segovia, J. L. *Vacuum* **1990**, *41*, 40.

(35) Onishi, H.; Aruga, T.; Egawa, C.; Iwasawa, Y. *Surf. Sci.* **1988**, *193*, 33.

(36) Wiesendanger, R. *Scanning Probe Microscopy and Spectroscopy: Methods and Applications*; Cambridge University Press: New York, 1994.

(37) Diebold, U.; Anderson, J. F.; Ng, K.-O.; Vanderbilt, D. *Phys. Rev. Lett.* **1996**, *77*, 1322.

(38) Jones, F. H.; Rawlings, K.; Foord, J. S.; Cox, P. A.; Egdell, R. G.; Pethica, J. B.; Wanklyn, B. M. R. *Phys. Rev. B* **1995**, *52*, R14392.

(39) Tanner, R. E.; Meethunkij, P.; Altman, E. I. *J. Phys. Chem. B* **2000**, *104*, 12315.

(40) Fukui, K.; Onishi, H.; Iwasawa, Y. *Chem. Phys. Lett.* **1997**, *280*, 296.

(41) Chambers, S. A.; Thevuthasan, S.; Kim, Y. J.; Herman, G. S.; Wang, Z.; Tober, E.; Ynzunza, R.; Morais, J.; Peden, C. H. F.; Ferris, K.; Fadley, C. S. *Chem. Phys. Lett.* **1997**, *267*, 51.

(42) Guo, Q.; Cocks, I.; Williams, E. M. *J. Chem. Phys.* **1997**, *106*, 2924.

(43) Yin, X.; Miura, R.; Endou, A.; Gunji, I.; Yamauchi, R.; Kubo, M.; Stirling, A.; Fahmi, A.; Miyamoto, A. *Appl. Surf. Sci.* **1997**, *119*, 199.

(44) Schelling, P. K.; Yu, N.; Halley, J. W. *Phys. Rev. B* **1998**, *58*, 1279.

(45) Rohrer, G. S.; Henrich, V. E.; Bonnell, D. A. *Science* **1990**, *250*, 1239.

(46) Nörenberg, H.; Tanner, R. E.; Schierbaum, K. D.; Fischer, S.; Briggs, G. A. D. *Surf. Sci.* **1998**, *396*, 52.

(47) Bennett, R. A.; Poulston, S.; Stone, P.; Bowker, M. *Phys. Rev. B* **1999**, *59*, 10341.

(48) Hyde, B. G.; Andersson, S. *Inorganic Crystal Structures*; Wiley Interscience: New York, 1989.

(49) Hyde, B. G.; Bagshaw, A. N.; Andersson, S.; O'Keeffe, M. *Ann. Rev. Mater. Sci.* **1974**, *4*, 43.

(50) Takakusagi, S.; Fukui, K.; Nariyuki, F.; Iwasawa, Y. *Surf. Sci.*, **2003**, *77*, L41.

**2003**, *523*, L41-L46.

(51) Guo, Q.; Cocks, I.; Williams, E. M. *Phys. Rev. Lett.* **1996**, *77*, 3851.

(52) Ashino, M.; Sugawara, Y.; Morita, S.; Ishikawa, M. *Phys. Rev. Lett.* **2001**, *86*, 4334.

(53) Ng, K.-O.; Vanderbilt, D. *Phys. Rev. B* **1997**, *56*, 10544.

(54) Sakama, H.; Kunimatsu, D.; Kageshima, M.; Kawazu, A. *Phys. Rev. B* **1996**, *53*, 6927.

(55) Dabrowski, J.; Mussig, H.-J.; Wolff, G. *Surf. Sci.* **1995**, *331-333*, 1022.

(56) Dabrowski, J.; Mussig, H.-J.; Wolff, G. *Phys. Rev. Lett.* **1994**, *73*, 1660.

**Table 4.1** Total number of unsaturated ligand coordination of exposed Ti atoms and the number of fourfold and fivefold coordinated Ti atoms per a unit cell of a bulk-terminated {114}-faceted structure for three surface structures as barometers of surface stability.

| | Number of exposed Ti atoms | | Total number of unsaturated coordination of exposed Ti atoms |
|---|---|---|---|
| | fourfold | fivefold | |
| Bulk-terminated (001) structure | 4 | 0 | 8 |
| Bulk-terminated {114}-faceted structure | 3 | 2 | 8 |
| Bleachers-like structure with added rows (Figure 4.9) | 1 | 3 | 5 |

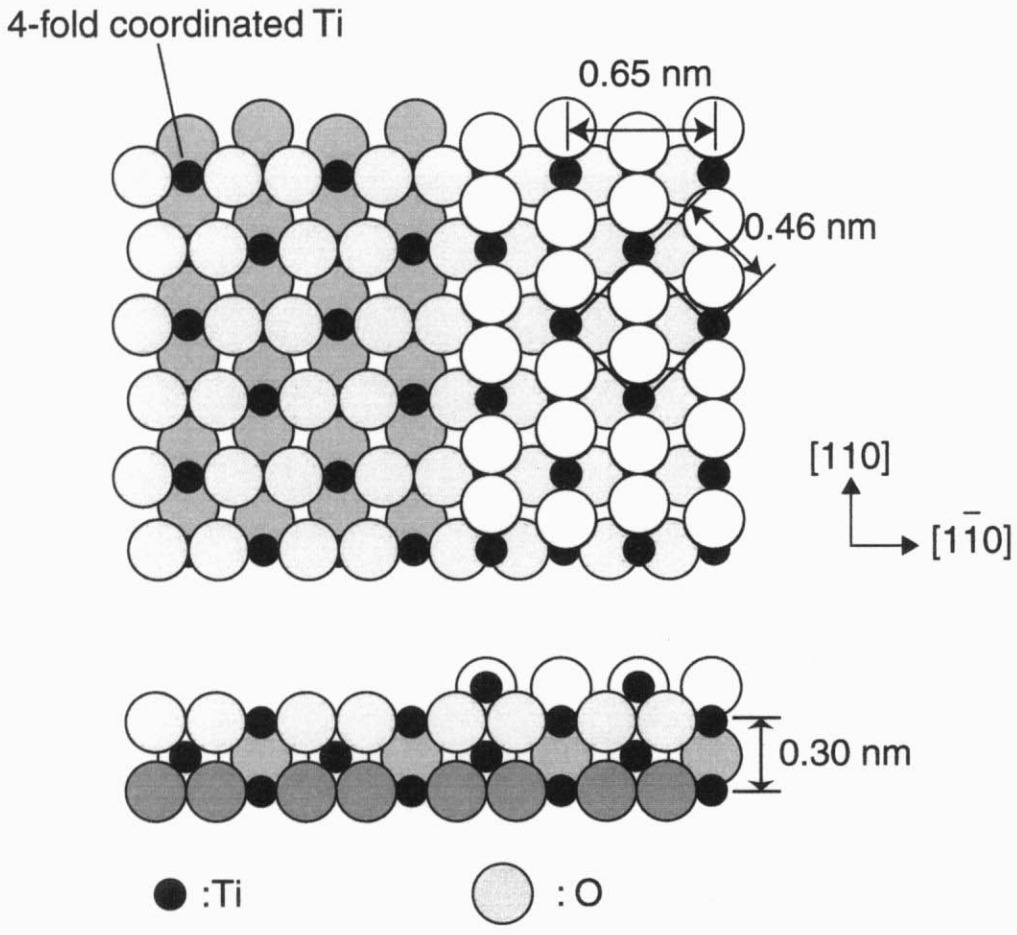


**Figure 4.1**

Bulk-terminated structural model of a rutile $TiO_2(001)$ surface which includes a half-height step along the [110] direction. Small black circles and gray large circles represent titanium and oxygen atoms, respectively.

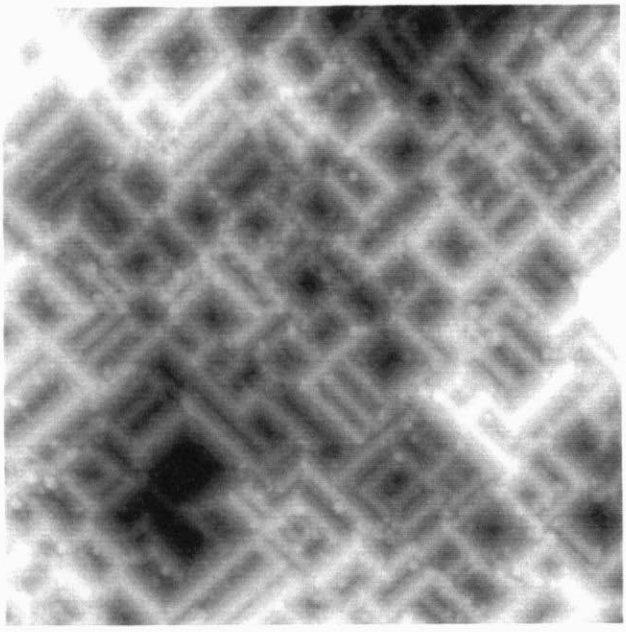


**Figure 4.2**

Constant current topograph (CCT) (100x100 $nm^2$, $V_s$: +2.0 V, $I_t$: 0.02 nA) of a $TiO_2$(001) surface after annealing an $Ar^+$-ion-sputtered surface at 1050 K for 5 min.

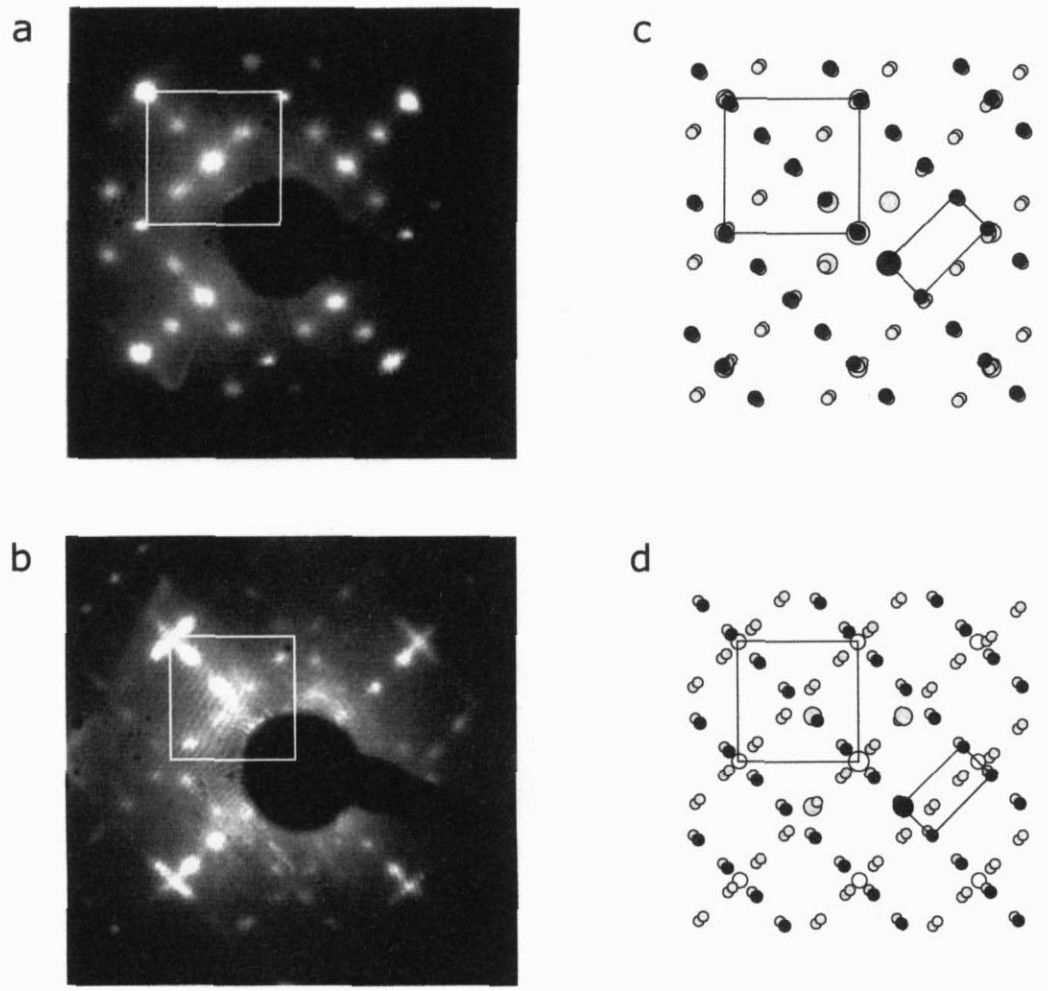


**Figure 4.3**

(a), (b) LEED patterns of the bleachers-like structure on $TiO_2$(001) simultaneously obtained with figure 4.2 with incident beam energy of (a) 43.0 eV, (b) 55.3 eV.

(c), (d) Predicted LEED patterns from bulk-terminated (114) structure. Empty and filled circles represented (001) substrate and (114) overlayer, respectively, and the square and rectangular are each unit cell. Larger circles represented specular spots of each pattern. One of four equivalent (114) patterns was drawn in black and other three were in gray.

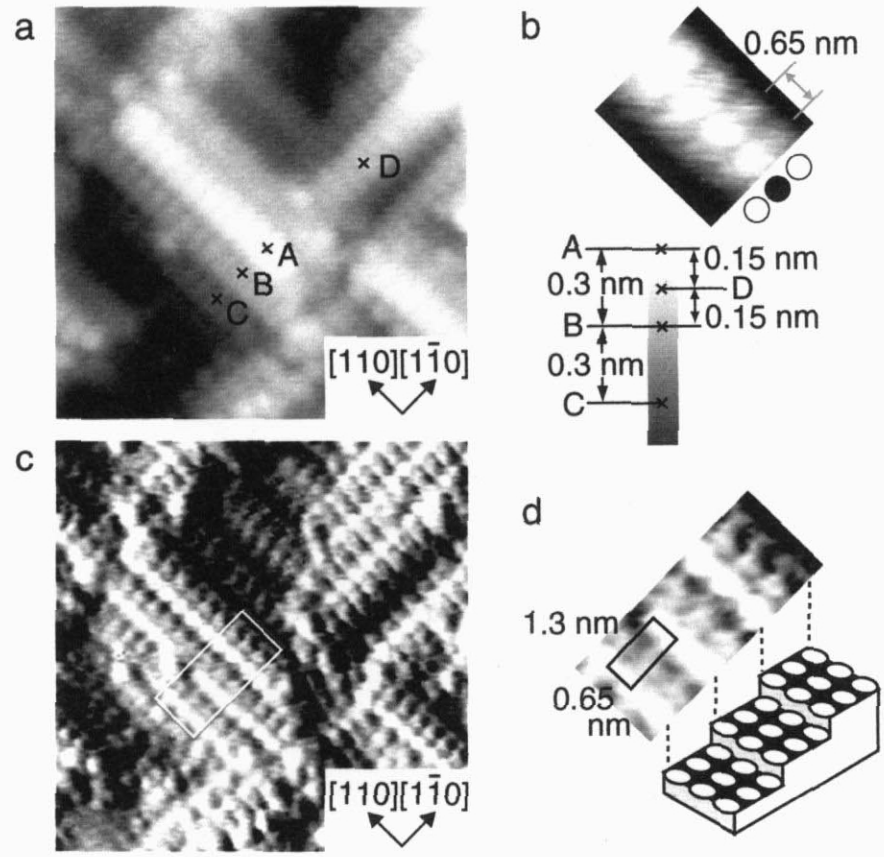


**Figure 4.4**

Atom-resolved STM images of a bleachers-like structure on $TiO_2$(001):

(a) a CCT image (15x15 $nm^2$, $V_s$: +2.0 V, $I_t$: 0.20 nA).

(b) a magnified image (2.6x2.3 $nm^2$, $V_s$: +2.0 V, $I_t$: 0.14 nA) of the topmost terrace in (a).

(c) a variable current image (15x15 $nm^2$, $V_s$: +2.0 V, $I_t$: ~0.15 nA) at the same area as (a).

(d) A magnified image of the rectangular area in (c) and schematic drawing showing the relative position of the bright spots.

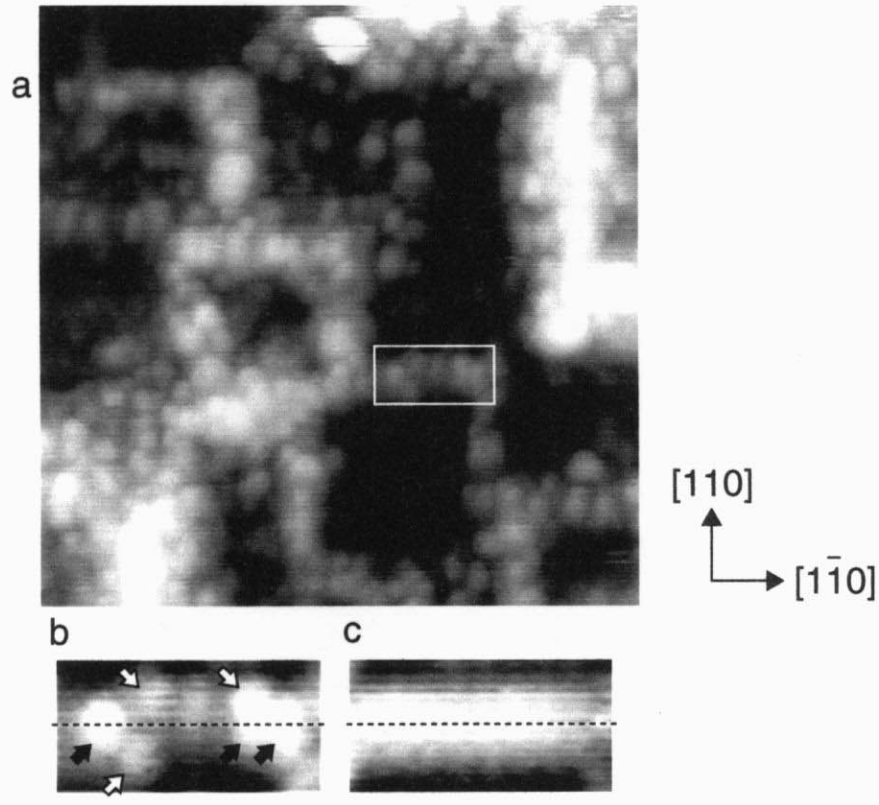


**Figure 4.5**

(a) CCT (30x30 $nm^2$, $V_s$: +2.0 V, $I_t$: 0.2 nA) of a latticework structure on $TiO_2$(001) after exposure to 12 L of formic acid at RT. Each adsorbed formate ion was imaged as a bright protrusion on the row-structure.

(b) Magnified image of the rectangular area in (a) (6.0x3.0 $nm^2$)

(c) CCT ($V_s$: +1.0 V, $I_t$: 0.50 nA) at the same area as (b) before exposure to formic acid as a reference.

Dotted lines in (b) and (c) indicate the row of center-bright spots at the top of the row. Black and white arrows in (b) indicate adsorbed formates on center-bright spots and side-bright spots, respectively.

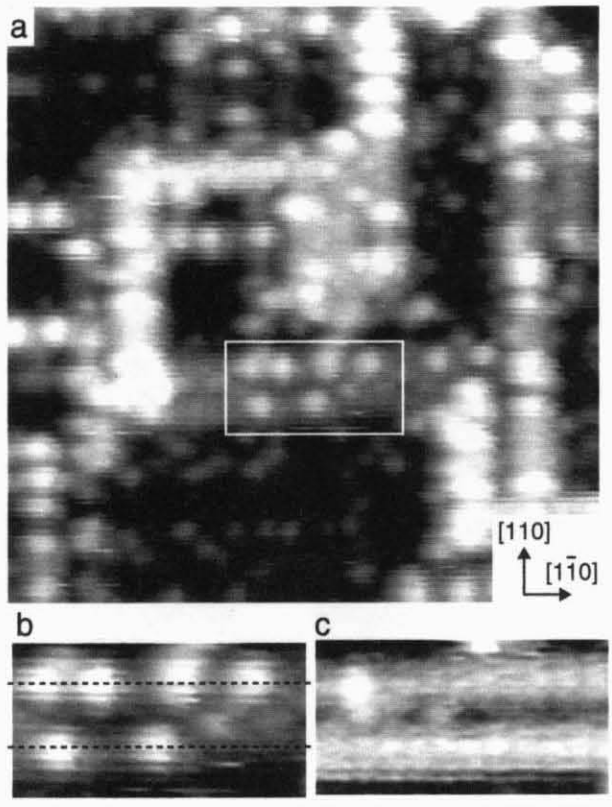


**Figure 4.6**

(a) CCT (24x24 $nm^2$, $V_s$: +1.2 V, $I_t$: 0.02 nA) of a bleachers-like structure on $TiO_2$(001) after exposure to 3.0 L of methanol at RT. Each adsorbed methoxy species was imaged as a bright protrusion on the row-structure.

(b) Magnified image of the rectangular area in (a) (6.8x3.6 $nm^2$).

(c) CCT (6.8x3.6 $nm^2$, $V_s$: +2.0 V, $I_t$: 0.06 nA) at the same area as (b) before exposure to methanol as a reference. Note that the image contrast in (c) is much higher than that in (b) to enhance the contrast difference of top narrow terrace. Then the bright spots, which may be structural defects, in (c) are much lower than methoxy and cannot be recognized in (b). Dotted lines in (b) and (c) indicate the rows of center-bright spots at the top terraces of two parallel rows. The two narrow terraces were the same height and were separated by a narrow terrace which was 0.30 nm lower than them.

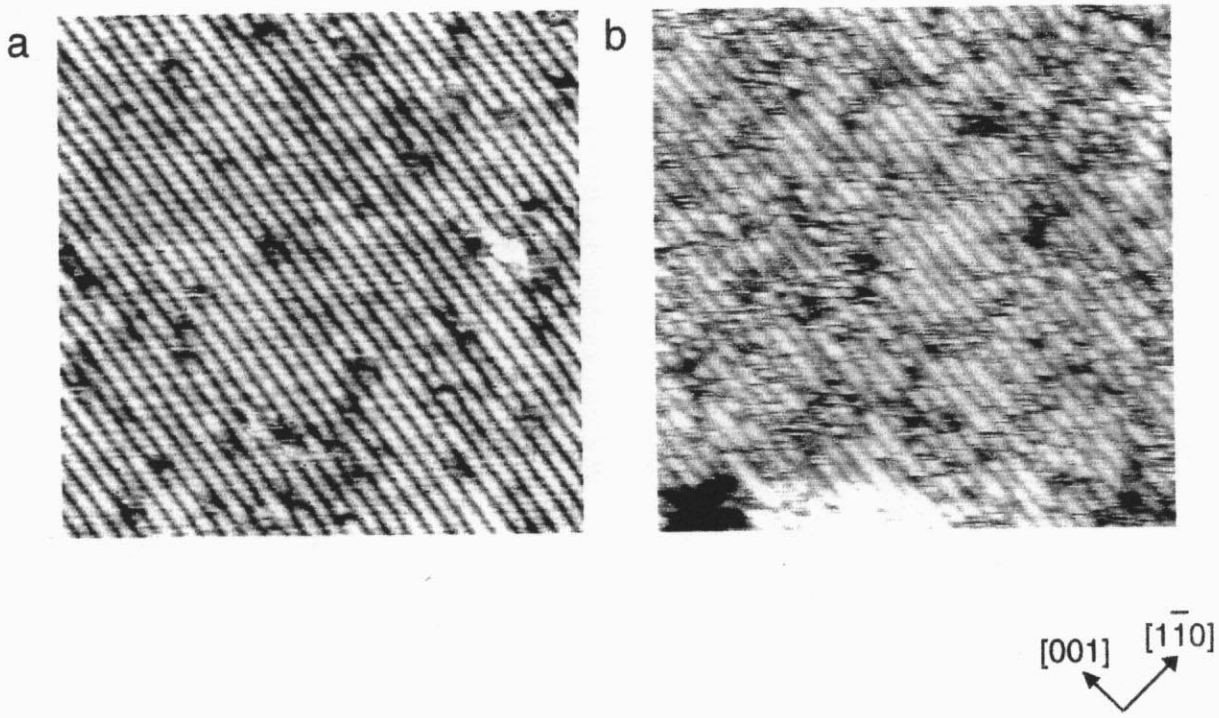


**Figure 4.7**

CCTs (20x20 $nm^2$) of $TiO_2$(110)-(1x1) suface (a) before and (b) after exposure to 33 L of methanol at RT. (a) $V_s$: 2.0 V, $I_t$, 0.11 nA, (b) $V_s$: 2.0 V, $I_t$, 0.10 nA. Each images were obtained at not the same but near regions.

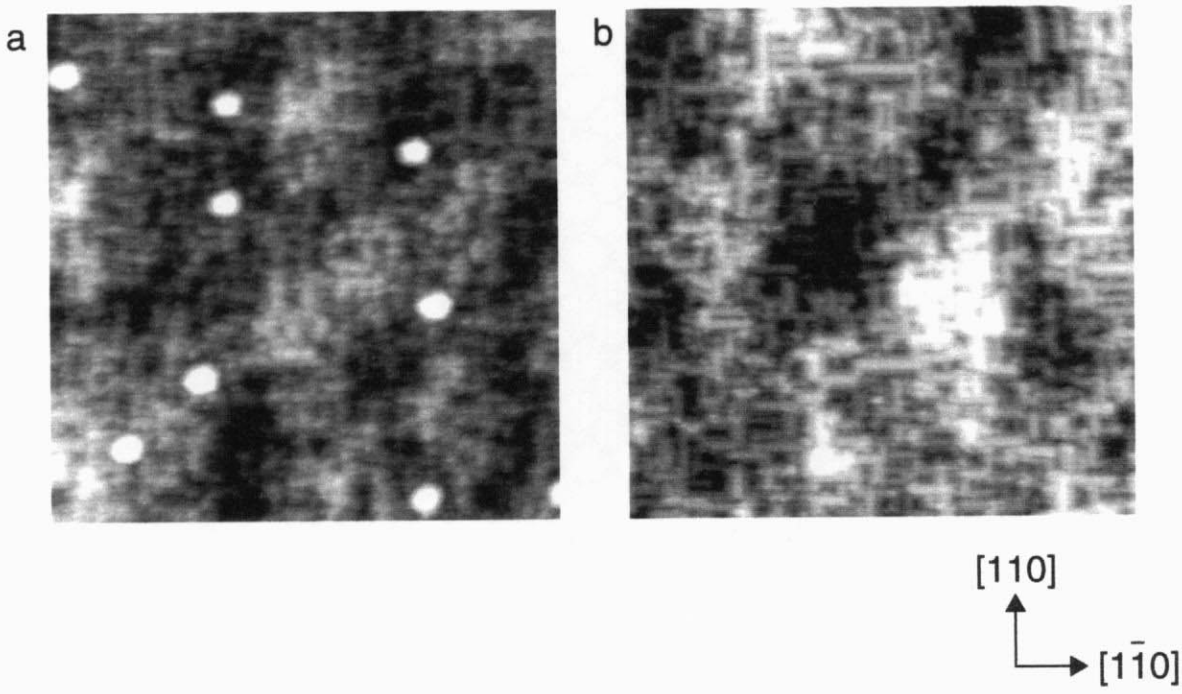


**Figure 4.8**

CCT images (80x80 $nm^2$) of the bleachers-like structure on $TiO_2$(001) after adsorption and thermal reaction of formic acid or methanol.

The clean bleachers-like structure was exposure to (a) 12 L of formic acid (Vs: +2.0 V, It: 0.05 nA) and (b) 48 L of methanol (Vs: +2.0 V, It: 0.03 nA) at RT, respectively and annealed to 700 K. Note that the surface structure is mostly preserved even after such thermal reactions while some protrusions were observed in (a) with a low density.

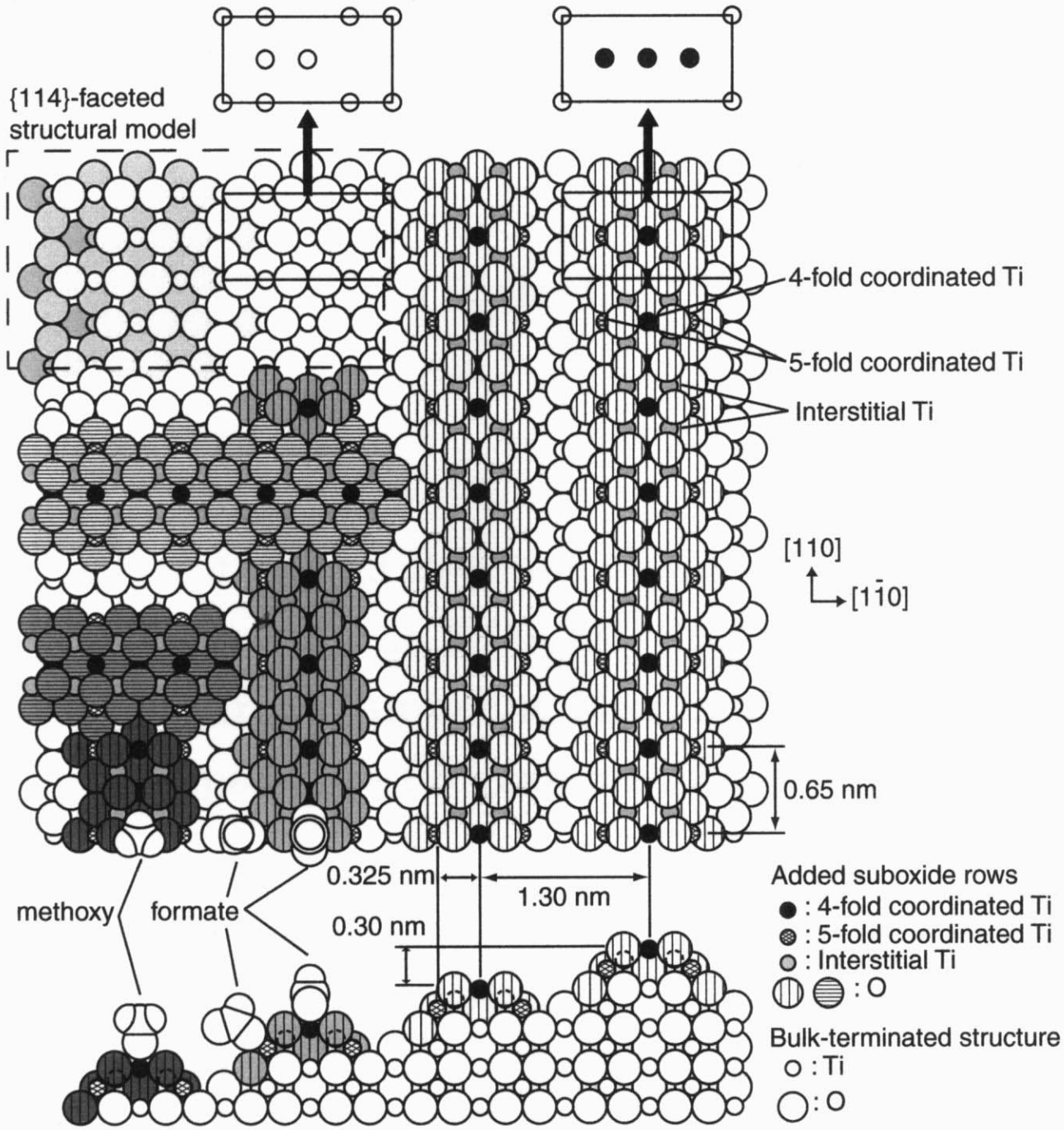


**Figure 4.9**

Structural model (top and side view) of the latticework structure on $TiO_2$(001). Suboxide rows are added on the bulk-terminated (1x1) structure. The added rows are crossed with one another at lower left region. Previously proposed {114}-faceted structural model is also displayed at the upper left for comparison. Position of coordinatively unsaturated Ti atoms in a unit cell of the two structural models are picked up at the top of the figure. Small and large empty circles represent Ti and O atoms in a bulk crystal, respectively. Filled, shaded and gray small circles represent fourfold coordinated, fivefold coordinated and interstitial Ti atoms in the added suboxide rows, respectively. Shadings were used for the added rows and {114}-faceted region to clarify the height differences between them. Adsorbed formate and methoxy species are also drawn at lower left in the figure, where corresponding van der Waals spheres are postulated for each atom.